

NUMERICAL STUDY OF BROWNIAN MOTION AND THERMOPHORESIS ON FREE CONVECTION IN A TRAPEZOIDAL ENCLOSURE USING BUONGIORNO'S NANOFLUID MODEL

By

Shatay Khatun

Student No. **1017093012**

Session: October'2017


M. Phil
IN
MATHEMATICS




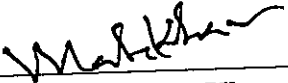
Department of Mathematics
BANGLADESH UNIVERSITY OF ENGINEERING AND TECNOLOGY
DHAKA-1000
June, 2021

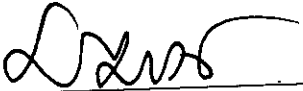
The thesis entitled "NUMERICAL STUDY OF BROWNIAN MOTION AND THERMOPHORESIS ON FREE CONVECTION IN A TRAPEZOIDAL ENCLOSURE USING BUONGIORNO'S NANOFUID MODEL", submitted by Shatay Khatun, roll no: 1017093012, Registration No. 1017093012, Session October-2017 has been accepted as satisfactory in partial fulfillment of the requirement for the degree of M.Phil. in Mathematics on 7th June, 2021.


Board of Examiners

1. 

Dr. Rehena Nasrin
Professor
Department of Mathematics
BUET, Dhaka-1000
**Chairman
(Supervisor)**
2. 

Dr. Khandker Farid Uddin Ahmed
Professor and Head
Department of Mathematics
BUET, Dhaka-1000
**Member
(Ex-Officio)**
3. 

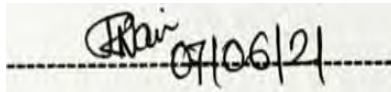
Dr. Md. Abdul Hakim Khan
Professor
Department of Mathematics
BUET, Dhaka-1000
Member
4. 

Dr. Md. Manirul Alam Sarker
Professor
Department of Mathematics
BUET, Dhaka-1000
Member
5. 

Dr. Md. Yeakub Ali
Professor
Department of Mathematics
CUET, Chittagong-4349
**Member
(External)**

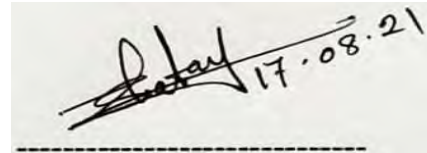
Certificate of Research

This is to certify that the work presented in this thesis has been carried out by the author under the supervision of **Dr. Rehana Nasrin**, Professor, Department of Mathematics, Bangladesh University of Engineering and Technology, Dhaka-1000.



Rehan 07/06/21

Dr. Rehana Nasrin
Professor
Dept. of Mathematics
BUET, Dhaka-1000

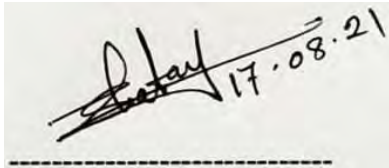


Shatay 17.08.21

Shatay Khatun

Candidate's Declaration

It is hereby declared that this thesis or any part of it has not been submitted elsewhere for the award of any degree or diploma.

A photograph of a handwritten signature and date on a piece of paper. The signature is written in black ink and appears to be 'Shatay'. To the right of the signature, the date '17.08.21' is written. The paper is slightly tilted.

Shatay Khatun

This work is dedicated
To
My Mother

Acknowledgement

I would like to affirm the continual mercy, help and blessing showered by the Almighty without which it would have been impossible to accomplish the arduous job I was assigned to.

With my great pleasure I would like to express my deep and sincere gratitude to my respected supervisor **Dr. Rehana Nasrin**, Professor, Department of Mathematics, Bangladesh University of Engineering and Technology, Dhaka-1000 for her expert guidance and valuable suggestions throughout this work. Her priceless suggestions made this work interesting and learning to me. It would not have been possible to carry out this study successfully without the continuous inspiration and encouragement from supervisor.

My special thanks to the **Head**, Department of Mathematics, BUET, for his support in allowing me to use the departmental facilities in various stages of my work. I also thank the staffs of the Department of Mathematics, BUET for being so helpful.

I would like to take the opportunity to gratitude and profound respect to, **Dr. Md. Abdul Hakim Khan**, Professor, Department of Mathematics, BUET for his comments and constructive concept which helped me for better understanding the issues of this thesis.

I also like to thank and profound respect to, **Dr. Md. Manirul Alam Sarker**, Professor, Department of Mathematics, BUET for his giving me valuable ideas, suggestions and inspiration to complete my thesis.

I am indebted to the **External Member** of the Board of Examiners for his valuable suggestions in upgrading the quality of the work.

Finally, I would like to express my gratitude to my family member for their steadfast love and support. They have kept me going through the most difficult times. I truly thank my family members for keeping faith in my quirkiness and intellect as well as sticking by my side, even when I was irritable and depressed.

Abstract

In this thesis, a numerical analysis has been carried out on free convection in a trapezoidal enclosure with sinusoidal temperature distributions on both side walls using Buongiorno's model. The model takes into account the Brownian motion and thermophoresis effect on the flow, temperature, and concentration fields. Non-uniform temperature and nanoparticle volume fraction distributions have been imposed on both inclined surfaces. Top and bottom parallel surfaces have been kept as adiabatic. All the walls will be considered no slip and impermeable. The governing equations along with above boundary conditions have been initially transformed into non-dimensional form using appropriate similarity transformation and then solved numerically, employing the finite element method of Galerkin's weighted residual approach. The code validation will be carried out. Nanofluids on the flow structure and heat transfer characteristics will be investigated in details. Results will be presented in terms of streamlines, isothermal lines and iso-concentration lines for different values of governing parameters such as Lewis number (Le), Brownian motion (Nb), Buoyancy ratio (Nr), Prandtl number (Pr), thermophoresis (Nt) and Rayleigh number (Ra). The effect of Brownian motion and thermophoresis on the fluid flow, temperature, and concentration will be identified and finally the flow, heat and concentration controlling parameters for a specific heat and mass transfer application in a trapezium shaped cavity will be obtained. Result demonstrates that, the increase of Brownian motion leads to increase in average Nusselt number by 34.75% and 34.27% for the right and left walls, respectively.

Contents

Abstract	vii
Nomenclature	x
List of Tables	xii
List of Figures	xiii
Chapter 1: Introduction	1
1.1.1 Buongiorno's model	1
1.1.2 Nanofluid	2
1.1.3 Sinusoidal temperature	3
1.1.4 Free convection	4
1.1.5 Buoyancy ratio	4
1.1.6 Lewis number	5
1.1.7 Prandtl number	6
1.1.8 Nusselt number.....	6
1.1.9 Rayleigh number	7
1.1.10 Thermophoresis	8
1.1.11 Brownian motion.....	9
1.1.12 Viscosity	11
1.1.13 Thermal conductivity.....	12
1.1.14 Density	12
1.2 Literature Review.....	13
1.3 Objectives	16
1.4 Scope of the Thesis.....	17
Chapter 2: Numerical Study of Buongiorno's Nanofluid Model.....	18
2.1. Introduction	18
2.2. Finite Element Method	18
2.3. Galerkin's Technique	20
2.4. Physical Model	21
2.5 Mathematical Model	22

2.6 Computational Procedure.....	25
2.6.1 Code validation.....	26
2.6.2 Mesh generation.....	27
2.6.3 Grid sensitivity test.....	28
Chapter 3: Results and Discussions.....	29
3.1 Introduction.....	29
3.2 Effect of Lewis Number.....	29
3.3 Effect of Thermophoresis.....	32
3.4 Effect of Prandtl Number.....	34
3.5 Effect of Brownian Motion.....	36
3.6 Effect of Buoyancy Ratio.....	38
3.7 Effect of Rayleigh Number.....	41
3.8 Comparison.....	43
Chapter 4: Conclusions and Recommendations	45
4.1 Conclusions.....	45
4.2 Recommendations.....	46
References.....	47

Nomenclature

C_p	Concentration ($mol.m^{-3}$)
C	Specific heat at constant pressure ($Jkg^{-1}K^{-1}$)
D	Diffusion coefficient (m^2s^{-1})
G	Gravitational force (ms^{-2})
h	Local convective heat transfer coefficient
H	Reference height (m)
K	Thermal conductivity ($Wm^{-1}K^{-1}$)
Le	Lewis Number
n	Dimensional distance
N	Dimensionless distance
Nb	Brownian motion parameter
Nr	Buoyancy ratio parameter
Nt	Thermophoresis Number
Nu	Average Nusselt number
P	Pressure ($kgms^{-2}$)
Pr	Prandtl number
Ra	Rayleigh number
T	Dimensional temperature (K)
u, v	Dimensional x and y components of velocity (ms^{-1})
U, V	Dimensionless velocities
x, y	Cartesian coordinates (m)
X, Y	Dimensionless coordinates

Greek Symbols

β	Coefficient of thermal expansion ($1/K$)
ρ	Density (kgm^{-3})
θ	Dimensionless temperature
μ	Dynamic viscosity (Nsm^{-2})
ψ	Stream function
α	Thermal diffusivity (m^2/s)
φ	Dimensionless concentration
ε	Dimensionless amplitude

Subscripts

c	Cold
h	Hot
f	Fluid

Abbreviation

FEM	Finite element method
HTF	Heat transferring fluid
MHD	Magnetohydrodynamic

List of Tables

Items	Table Caption	Page
Table 2.1	Grid sensitivity check at $Pr = 7$, $Ra = 10^4$, $Nt = Nr = Nb = 0.1$ and $Le = 10$.	28
Table 3.1	Comparison of Nu against Pr among present result and that of Demirdzic <i>et al.</i> [39] and Revnic <i>et al.</i> [5]	44
Table 3.2	Comparison of Nu against Ra among present result and that of Davis and Jones [40] and Revnic <i>et al.</i> [5]	44

List of Figures

Items	Figure Caption	Page
Figure 1.1	Formation of nanofluid	3
Figure 1.2	Undulated enclosure	3
Figure 1.3	Convection	4
Figure 1.4	Buoyancy ratio	5
Figure 1.5	Simulation of thermophoresis in nanofluids	9
Figure 1.6	Brownian movement – Collisions between Particles	10
Figure 1.7	Viscosity of honey	11
Figure 2.1	Physical model	22
Figure 2.2	Code validation of the streamlines and isotherms	26
Figure 2.3	Mesh generation of the trapezoidal enclosure	27
Figure 3.1	Effect of Lewis number on (a) streamlines, (b) isothermal lines and (c) iso-concentration lines at $Pr = 7$, $Ra = 10^4$, $Nt = Nr = Nb = 0.1$	30
Figure 3.2	Average Nusselt number at left and right wall against Lewis number at $Pr = 7$, $Ra = 10^4$, $Nt = Nr = Nb = 0.1$	31
Figure 3.3	Effect of thermophoresis parameter on (a) streamlines, (b) isothermal lines and (c) iso-concentration lines at $Le = 10$, $Pr = 7$, $Ra = 10^4$, $Nr = Nb = 0.1$	33
Figure 3.4	Average Nusselt number at left and right wall against thermophoresis parameter at $Pr = 7$, $Ra = 10^4$, $Nr = Nb = 0.1$	34
Figure 3.5	Effect of Prandtl number on (a) streamlines, (b) isothermal lines and (c) iso-concentration lines at $Ra = 10^4$, $Nt = Nr = Nb = 0.1$ and $Le = 10$	35
Figure 3.6	Average Nusselt Number at the left and right walls against Prandtl number at $Le = 10$, $Ra = 10^4$, $Nt = Nr = Nb = 0.1$	36
Figure 3.7	Effect of Brownian motion on ((a) streamlines, (b) isothermal lines and (c) iso-concentration lines at $Pr = 7$, $Ra = 10^4$, $Nt = Nr = 0.1$, $Le = 10$	37
Figure 3.8	Average Nusselt number at the left and right walls against Brownian motion at $Pr = 7$, $Ra = 10^4$, $Nt = Nr = 0.1$, $Le = 10$	38
Figure 3.9	Effect of buoyancy ratio on (a) streamlines, (b) isothermal lines and (c) iso-	39

concentration lines at $Pr = 7$, $Ra = 10^4$, $Nt = Nb = 0.1$, $Le = 10$

Figure 3.10 Average Nusselt Number at the left and right walls against buoyancy ratio at 40
 $Le = 10$, $Ra = 10^4$, $Pr = 7$, $Nt = Nb = 0.1$

Figure 3.11 The effect of Rayleigh number on (a) streamlines, (b) isothermal lines and (c) 42
iso-concentration lines at $Pr = 7$, $Nt = Nr = Nb = 0.1$, $Le = 10$

Figure 3.12 Average Nusselt number at the left and right walls against Rayleigh number at 43
 $Le = 10$, $Ra = 10^4$, $Nt = Nr = Nb = 0.1$

Chapter 1: Introduction

1.1. Introduction

One of the proficient passive approaches is using nanofluid in heat transport improvement for enhancing the efficiency of thermal systems like heat exchangers, thermal storage, solar collectors, photovoltaic/thermal system, biomedical devices, nuclear reactors, cooling of electronic components etc. Researches on the nanofluids have been increased very rapidly over the past decade.

It is observed that few researches have been done using Buongiorno's model. In spite of this research, more investigations are still needed especially for Brownian motion and thermophoresis effect on flow, temperature and concentration fields due to their huge applications. The Buongiorno's model is able to consider the effect of nanoparticle volume fraction distribution. This model can also explore the heat transfer phenomena caused by Brownian motion and thermophoresis by using similarity transformations.

In spite of some inconsistency in the reported results and insufficient understanding of the mechanism of the heat transfer in nanofluids, it has been emerged as a promising heat transfer fluid. In the continuation of nanofluids research, the researchers have also tried to use nanofluid recently, which is engineered by suspending dissimilar nanoparticles either in mixture or composite form. The idea of using nanofluids is to further improvement of heat transfer and pressure drop characteristics by trade-off between advantages and disadvantages of individual suspension, attributed to good aspect ratio, better thermal network and synergistic effect of nanomaterials.

1.1.1 Buongiorno's model

The Buongiorno model assumes that the nanofluid is a mixture of a base fluid and nanoparticles, with the relative motion caused by Brownian motion and thermophoretic diffusion. The Buongiorno's model is able to consider the effect of nanoparticle volume fraction distribution. Buongiorno model is used to explore the heat transfer phenomena caused by Brownian motion and thermophoresis. In the recent year convection of nanofluid using Buongiorno's model has

received considerable attention because of its relation to the thermal performance of many engineering installations. Buongiorno's model might be useful for designing the solar collectors, room ventilation system, and electronic cooling system. In this paper the flow, heat and concentration controlling parameters for a specific heat and mass transfer application in a trapezium shaped cavity will be obtained by applying this model.

1.1.2 Nanofluid

A nanofluid is a fluid containing nanometer-sized particles, called nanoparticles (1-100 nm). These fluids are engineered colloidal suspensions of nanoparticles in a base fluid. Many types of nanoparticles such as metals (Cu, Ag, Au), oxide ceramics (Al_2O_3 , CuO), carbon nanotubes and carbide ceramics (SiC, TiC) and various liquids such as water, oil, and ethylene glycol are used. The fundamental characteristics of the nanofluid are the raise of the thermal conductivity of the fount fluid, minimal impeding in flow passing, extensive stability and equity. Nanofluids have novel properties that make them potentially useful in many applications in heat transfer including microelectronics, fuel cells, pharmaceutical processes, and hybrid-powered engines, engine cooling/vehicle thermal management, domestic refrigerator, chiller, heat exchanger, in grinding, machining and in boiler flue gas temperature reduction. They exhibit enhanced thermal conductivity and the convective heat transfer coefficient compared Nanofluids also have special acoustical properties and in ultrasonic fields display additional shear-wave reconversion of an incident compressional wave; the effect becomes more pronounced as concentration increases. There have been numerous investigations that have revealed the enhancement of thermal conductivity and higher heat transfer rate of nanofluids. Significant enhancement in the heat transfer rate with the use of various nanofluids in various application compared to conventional fluids have been reported by several researchers. Understanding the properties of nanofluids, such as thermal conductivity, viscosity and specific heat, is very important for the utilization of nanofluids in various applications. Further study of the fundamentals for heat transfer and friction factors in the case of nanofluids is considered to be very important in order to extend the applications of nanofluids. Figure 1.1 displays the formation of nanofluid.

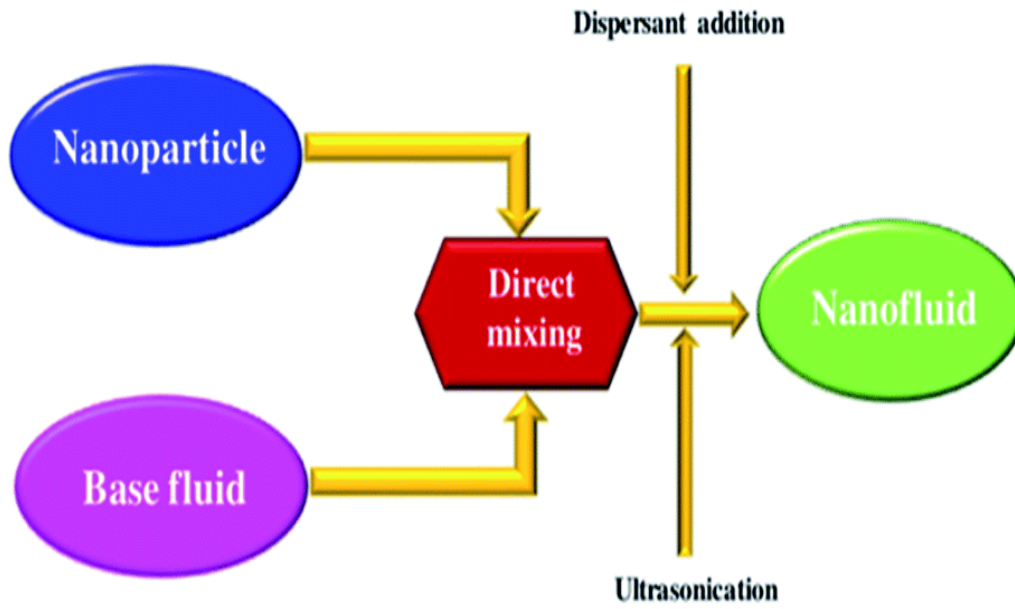


Figure 1.1: Formation of nanofluid

1.1.3 Sinusoidal temperature

Graphs of sine and cosine functions are called sinusoids. The temperature in a wavy form is called sinusoidal temperature and the way of distribution is known as sinusoidal temperature distribution. In many numerical analyses of the convection of nanofluid the temperature is taken sinusoidal. Figure 1.2 shows the undulated temperature at inclined walls.

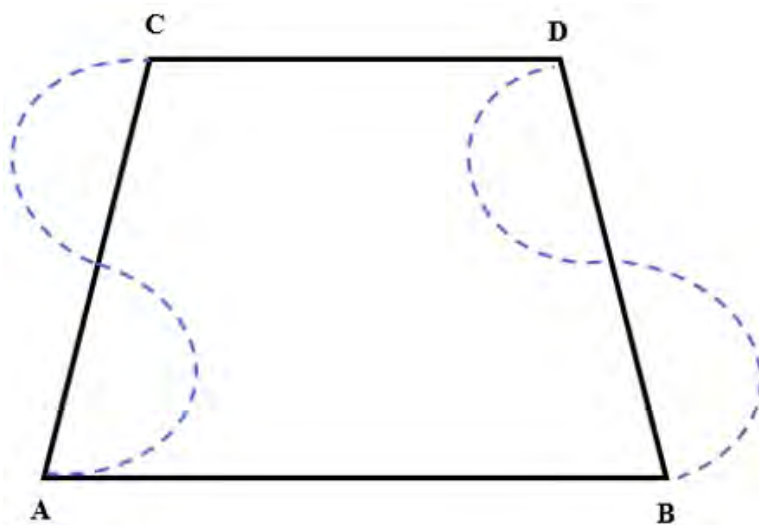


Figure 1.2: Undulated temperature at inclined walls

1.1.4 Free convection

Natural convection, known also as free convection is a mechanism, or type of mass and heat transport, in which the fluid motion is generated only by density differences in the fluid occurring due to temperature gradients, not by any external source (like a pump, fan, suction device, etc.). Free-convective flows may be laminar and turbulent. A flow past a solid surface, the temperature of which is higher (lower) than that of the surrounding flowing medium, is the most widespread type of free convection. Figure 1.3 displays convection.

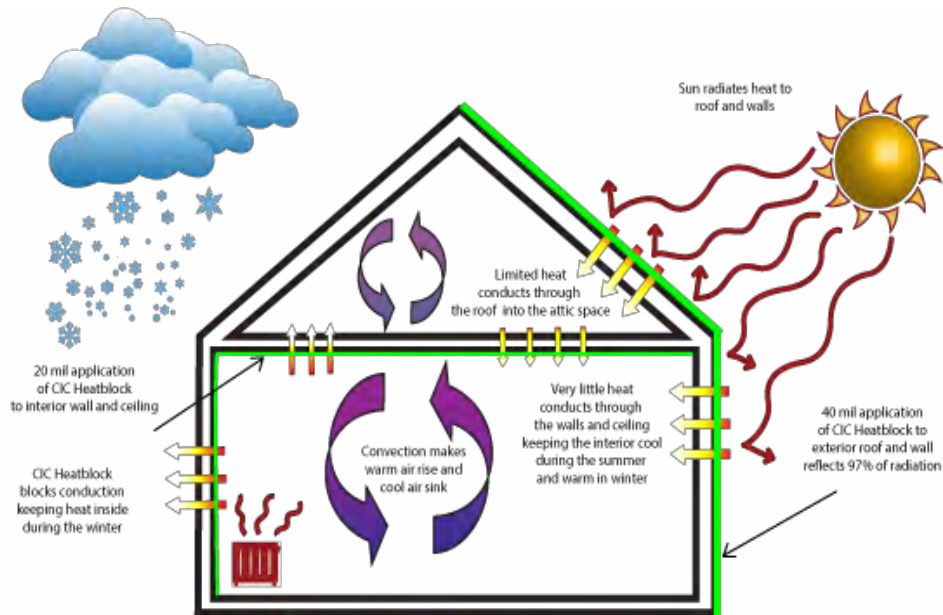


Figure 1.3: Convection

1.1.5 Buoyancy ratio

Buoyancy ratio can be expressed as the ratio of the specific weight of the fluid to the specific weight of the object; or, in another manner, by the weight of the fluid displaced minus the weight of the object.

The density of the immersed object relative to the density of the fluid can easily be calculated without measuring any volumes.

$$\frac{\text{density}}{\text{density of the fluid}} = \frac{\text{weight}}{\text{weight of the fluid}}$$

Buoyancy ratio shows the effect on heat and mass transfer on natural convection in a porous enclosure between two isothermal concentric cylinders of rhombic cross sections. For negative values of the buoyancy ratio, buoyancy forces due to heat and mass transfer are in opposite directions (opposing mode), while for positive values they are in the same direction (aiding mode). In this case, the flow strength increases as the absolute value of the buoyancy ratio increases. Figure 1.4 indicates Buoyancy ratio.

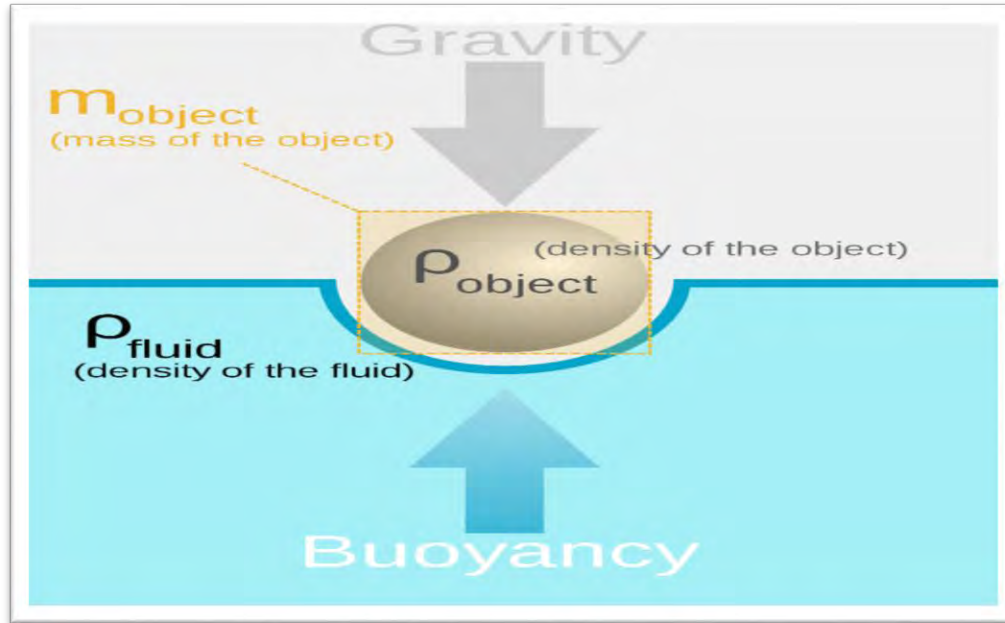


Figure 1.4: Buoyancy ratio

1.1.6 Lewis number

The Lewis number is a dimensionless number defined as the ratio of thermal diffusivity to mass diffusivity. It is used to characterize fluid flows where there is simultaneous heat and mass

transfer. It is defined as, $Le = \frac{\alpha}{D} = \frac{\lambda}{\rho D C_p}$

where α is the thermal diffusivity and D mass diffusivity, λ thermal conductivity, ρ the density, D mixture-averaged diffusion coefficient and the specific heat capacity at constant pressure.

1.1.7 Prandtl number

Prandtl number (Pr) or Prandtl group is a dimensionless number, named after the German physicist Ludwig Prandtl, defined as the ratio of momentum diffusivity to thermal diffusivity. That is, the Prandtl number is given as:

$$Pr = \nu / \alpha = \text{momentum diffusivity} / \text{thermal diffusivity} = \frac{\mu / \rho}{k / (C_p \rho)}$$

Where,

ν : momentum diffusivity (kinematic viscosity), $\nu = \mu / \rho$, (m^2/s)

α : thermal diffusivity, $\alpha = \frac{k}{(\rho C_p)}$, (m^2/s)

μ : dynamic viscosity, ($N \cdot s/m^2$)

k : thermal conductivity, ($W/m \cdot K$)

C_p : specific heat, ($J/kg \cdot K$)

ρ : Density, (kg/m^3).

Note that the Prandtl number contains no such length scale in its definition and is dependent only on the fluid and the fluid state. The Prandtl number is often found in property tables alongside other properties such as viscosity and thermal conductivity.

For most gases over a wide range of temperature and pressure, Pr is approximately constant. Therefore, it can be used to determine the thermal conductivity of gases at high temperatures, where it is difficult to measure experimentally due to the formation of convection currents.

1.1.8 Nusselt number

The Nusselt number is the ratio of convective to conductive heat transfer across a boundary. The convection and conduction heat flows are parallel to each other and to the surface, normal of the boundary surface and are all perpendicular to the mean fluid flow in the simple case.

$$Nu = \frac{\text{Convective heat transfer}}{\text{Conductive heat transfer}} = \frac{h}{\frac{k}{L}} = \frac{hL}{k}$$

Where h is the convective heat transfer coefficient of the flow, L is the characteristics length, k is the thermal conductivity. A Nusselt number close to one, namely convection and conduction of

similar magnitude, is characteristic of "slug flow" or "laminar flow". A value from 1 to 10 is characteristic of slug flow or laminar flow. A larger Nusselt number corresponds to more active convection, with [turbulent flow] typically in the 100 – 1000 range. The Nusselt number is named after Wilhelm Nusselt, who made significant contributions to the science of convective heat transfer.

1.1.9 Rayleigh number

The Rayleigh number (Ra) for a fluid is a dimensionless number associated with buoyancy-driven flow, also known as free or natural convection. It characterizes the fluid's flow regime: a value in a certain lower range denotes laminar flow; a value in a higher range, turbulent flow. Below a certain critical value, there is no fluid motion and heat transfer is by conduction rather than convection.

The Rayleigh number is defined as the product of the Grashof number, which describes the relationship between buoyancy and viscosity within a fluid, and the Prandtl number, which describes the relationship between momentum diffusivity and thermal diffusivity. Hence it may also be viewed as the ratio of buoyancy and viscosity forces multiplied by the ratio of momentum and thermal diffusivities. It is closely related to the Nusselt number. For most engineering purposes, the Rayleigh number is large, somewhere around 10^6 to 10^8 . It is named after Lord Rayleigh, who described the property's relationship with fluid behavior. The Rayleigh number describes the behavior of fluids (such as water or air) when the mass density of the fluid is non-uniform. The mass density differences are usually caused by temperature differences. Typically, a fluid expands and becomes less dense as it is heated. Gravity causes denser parts of the fluid to sink, which is called convection. Lord Rayleigh studied the case of Rayleigh-Benard convection. When the Rayleigh number, Ra , is below a critical value for a fluid, there is no flow and heat transfer is purely by conduction; when it exceeds that value, heat is transferred by natural convection. When the mass density difference is caused by temperature difference, Ra is, by definition, the ratio of the time scale for diffusive thermal transport to the time scale for convective thermal transport at speed.

$$Ra = \frac{\text{time scale for thermal transport via diffusion}}{\text{time scale for tharmal transport via convection at speed } u}$$

1.1.10 Thermophoresis

Thermophoresis (also thermomigration, thermodiffusion, the Sorret effect, or the Ludwig–Soret effect) is a phenomenon of mass transport driven by a temperature gradient. Thermophoresis in gas mixtures was first observed and reported by John Tyndall in 1870 and further understood by John Strutt (Baron Rayleigh) in 1882. Thermophoresis in liquid mixtures was first observed and reported by Carl Ludwig in 1856 and further understood by Charles Soret in 1879. Soret developed phenomenological equations describing the thermodiffusion. Thermodiffusion in solids can be described by considering the heat of transport for the jump from a neighboring lattice position into a vacancy caused by crystal defects. The thermophoretic force has a number of practical applications. This phenomenon can be applied in aerosol mixtures. The basis for applications is that, because different particle types move differently under the force of the temperature gradient, the particle types can be separated by that force after they've been mixed together, or prevented from mixing if they're already separated.

Impurity ions may move from the cold side of a semiconductor wafer towards the hot side, since the higher temperature makes the transition structure required for atomic jumps more achievable. The diffusive flux may occur in either direction (either up or down the temperature gradient), dependent on the materials involved. Thermophoretic force has been used in commercial precipitators for applications similar to electrostatic precipitators. It is exploited in the manufacturing of optical fiber in vacuum deposition processes. It can be important as a transport mechanism in fouling. Thermophoresis has also been shown to have potential in facilitating drug discovery by allowing the detection of a patten binding by comparison of the bound versus unbound motion of the target molecule. This approach has been termed microscale thermophoresis. Furthermore, thermophoresis has been demonstrated as a versatile technique for manipulating single biological macromolecules, such as genomic-length deoxyribonucleic acid (DNA) and human immunodeficiency virus (HIV) virus in micro- and nano-channels by means of light-induced local heating. Thermophoresis is one of the methods used to separate different polymer particles in field flow fractionation. Figure 1.5 displays the Simulation of thermophoresis in nanofluids.

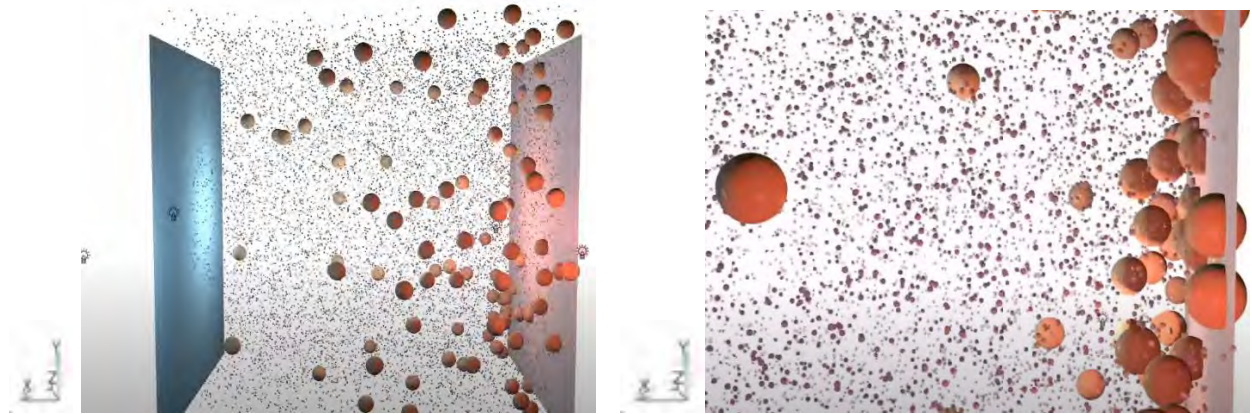


Figure 1.5: Simulation of thermophoresis in nanofluid

1.1.11 Brownian motion

Brownian motion refers to the random movement displayed by small particles that are suspended in fluids. It is commonly referred to as Brownian movement. Brownian motion is named after the Scottish Botanist Robert Brown, who first observed that pollen grains move in random directions when placed in water in 1827.

This motion is a result of the collisions of the particles with other fast-moving particles in the fluid. This pattern of motion typically alternates random fluctuations in a particle's position inside a fluid sub-domain with relocation to another sub-domain. Each re-location is followed by more fluctuations within the new closed volume. This pattern describes a fluid at thermal equilibrium, defined by a given temperature. Within such a fluid, there exists no preferential direction of flow as in transport phenomena. More specifically, the fluid's overall linear and angular momenta remain null over time.

In 1905, almost eighty years later, theoretical physicist Albert Einstein published a paper where he modeled the motion of the pollen as being moved by individual water molecules, making one of his first major scientific contributions. This explanation of Brownian motion served as convincing evidence that atoms and molecules exist and was further verified experimentally by Jean Perrin in 1908. Figure 1.6 displays Brownian motion of the Particles.

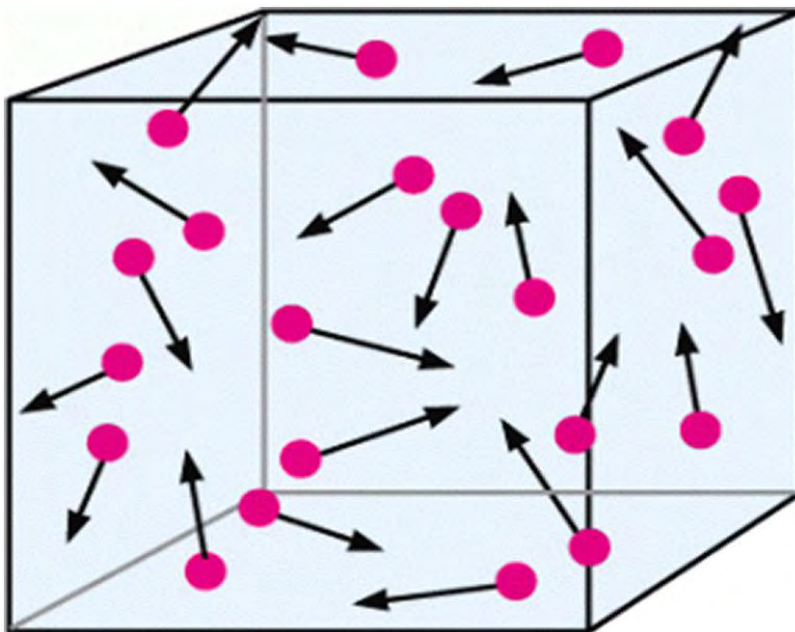


Figure 1.6: Brownian motion of the particles

Causes of Brownian motion

- The size of the particles is inversely proportional to the speed of the motion, i.e. Small particles exhibit faster movements.
- This is because the transfer of momentum is inversely proportional to the mass of the particles. Lighter particles obtain greater speeds from collisions.
- The speed of the Brownian motion is inversely proportional to the viscosity of the fluid. The lower the viscosity of the fluid, the faster the Brownian movement.
- Viscosity is a quantity that expresses the magnitude of the internal friction in a liquid. It is the measure of the fluid's resistance to flow.

Effects of Brownian motion

- Brownian movement causes the particles in a fluid to be in constant motion.
- This prevents particles from settling down, leading to the stability of colloidal solutions.
- A true solution can be distinguished from a colloid with the help of this motion.

1.1.12 Viscosity

The viscosity of a fluid is a measure of its resistance to deformation at a given rate. For liquids, it corresponds to the informal concept of "thickness": for example, syrup has a higher viscosity than water. Viscosity can be conceptualized as quantifying the internal frictional force that arises between adjacent layers of fluid that are in relative motion. For instance, when a fluid is forced through a tube, it flows more quickly near the tube's axis than near its walls. In such a case, experiments show that some stress (such as a pressure difference between the two ends of the tube) is needed to sustain the flow through the tube. This is because a force is required to overcome the friction between the layers of the fluid which are in relative motion: the strength of this force is proportional to the viscosity. A fluid that has no resistance to shear stress is known as an ideal or inviscid fluid. Zero viscosity is observed only at very low temperatures in super fluids. Otherwise, the second law of thermodynamics requires all fluids to have positive viscosity;^{[2][3]} such fluids are technically said to be viscous or viscid. A fluid with a high viscosity, such as pitch, may appear to be a solid. Figure 1.7 shows viscosity of honey.



Figure 1.7: Viscosity of honey

1.1.13 Thermal conductivity

Thermal conductivity refers to the amount/speed of heat transmitted through a material. Heat transfer occurs at a higher rate across materials of high thermal conductivity than those of low thermal conductivity. Materials of high thermal conductivity are widely used in heat sink applications and materials of low thermal conductivity are used in thermal insulation. Thermal conductivity of materials is temperature dependent. The reciprocal of thermal conductivity is called thermal resistivity. Metals with high thermal conductivity, e.g. copper exhibits high electrical conductivity. The heat generated in high thermal conductivity materials is rapidly conducted away from the region of the weld. For metallic materials, the electrical and thermal conductivity correlate positively, i.e. materials with high electrical conductivity (low electrical resistance) exhibit high thermal conductivity. The proportionality constant k is called thermal conductivity of the material.

1.1.14 Density

The density (more precisely, the volumetric mass density; also known as specific mass), of a substance is its mass per unit volume. The symbol most often used for density is ρ (the lower-case Greek letter rho), although the Latin letter D can also be used. Mathematically, density is defined as mass divided by volume:

$$\rho = \frac{m}{v}$$

Where m is the mass, and v is the volume. In some cases (for instance, in the United States oil and gas industry), density is loosely defined as its weight per unit volume, although this is scientifically inaccurate – this quantity is more specifically called specific weight. For a pure substance the density has the same numerical value as its mass concentration. Different materials usually have different densities, and density may be relevant to buoyancy, purity and packaging. Osmium and iridium are the densest known elements at standard conditions for temperature and pressure. To simplify comparisons of density across different systems of units, it is sometimes replaced by the dimensionless quantity "relative density" or "specific gravity", i.e. the ratio of the density of the material to that of a standard material, usually water. Thus, a relative density (less than one) means that the substance floats in water. The density of a material varies with temperature and pressure. This variation is typically small for solids and liquids but much greater

for gases. Increasing the pressure on an object decreases the volume of the object and thus increases its density. Increasing the temperature of a substance (with a few exceptions) decreases its density by increasing its volume. In most materials, heating the bottom of a fluid results in convection of the heat from the bottom to the top, due to the decrease in the density of the heated fluid. This causes it to rise relative to more dense unheated material.

1.2 Literature Review

One of the proficient passive approaches is using nanofluid in heat transport improvement for enhancing the efficiency of thermal systems like heat exchangers, thermal storage, solar collectors, photovoltaic/thermal system, biomedical devices, nuclear reactors, cooling of electronic components etc. The Buongiorno model is used to investigate the effects of Brownian motion and thermophoresis on the flow, heat, and mass transfer from a flat plate with prescribed surface heat flux.

Elshehabey and Ahmed [1] investigated MHD mixed convection in a lid driven cavity filled by nanofluid with sinusoidal temperature using Buongiorno's model. The effects of Brownian motion and thermophoresis are also incorporated into the nanofluids. The obtain result demonstrate that, the presence of an inclined magnetic field in the flow region leads to lose the fluid movement and also the fluid is dominated by the movement of the upper wall in the case of highest value of the buoyancy ratio. Sheikholeslami *et al.* [2] analyzed natural convection considering Brownian motion and thermophoresis effect. Their result indicated that Nusselt number is an increasing function of buoyancy ratio number but it is a decreasing function of Lewis number and Hartmann number. Suriyakumar and Devi [3] performed magneto-nanofluid flow including the effects of thermophoresis and Brownian motion numerically. Falana *et al.* [4] numerically studied the effect of Brownian motion and thermophoresis on a stretching sheet. Revnic *et al.* [5] showed the impact of border temperature variations on nanofluid free convection within a trapezium using Buongiorno's nanofluid model. They observed that Nusselt number is growing function of wave number and Rayleigh number.

Esfandiary *et al.* [6] conducted natural convective heat transfer considering Brownian motion and thermophoresis effect. The authors [7-8] found more accurate results using the Buongiorno's model compared to other nanofluid models. Behbahan and Pop [9] studied the thermophoresis

and Brownian effects on natural convection of nanofluids in a square enclosure with two pairs of heat source/sink. Their study showed an improvement in heat transfer rate for the whole range of Rayleigh numbers when Brownian and thermophoresis effects are considered.

Sheremet *et al.* [10] studied free convection in a shallow and slender porous cavity filled by a nanofluids. Elshehabe and Ahmed [11] numerically investigated MHD mixed convection in a lid driven cavity filled a nanofluid with sinusoidal temperature distribution on the vertical walls using Buongiorno's nanofluid model. Haddad *et al.* [12] studied the natural convection in nanofluids due to the effect of thermophoresis and Brownian motion in heat transfer enhancement. Matin and Ghanbari [13] studied the effect of Brownian motion and thermophoresis on the mixed convection of nanofluid in a porous channel including flow reversal. Aminfar and Haghgoo [14] investigated the effects of Brownian motion and thermophoresis effects on natural convection heat transfer of alumina-water nanofluid. They concluded that the use of single-phase homogeneous method does not seem reasonable for modeling this class of natural convection. Alsabery *et al.* [15] discussed the effect of spatial side-wall temperature variations on transient natural convection of a nonofluid in a trapezoidal cavity. The main object of this paper was to examine the effects of nonuniform border temperature variations on time dependent free nanofluid convection within a trapezium: Buongiorno's nanofluid model. Sheremet and pop [16] studied natural convection in square porous cavities with sinusoidal temperature distributions on both side walls filled with a nanofluid using Buongiorno's model. They applied the symmetric sinusoidal temperature with respect to the midplane of the enclosure.

Sivasankaran and Bhuvaneshwari [17] studied natural convection in porous cavity with sinusoidal heating on both sidewalls. Ho *et al.* [18] investigated the natural convection of Al_2O_3 -water nanofluid in square enclosure experimentally. They explained that the unusual increase or decrease of heat transfer cannot be explained on relative changes Malvandi *et al.* [19] analyzed thermophoresis and Brownian motion effect on heat transfer enhancement at film boiling of nanofluids. Garoosi *et al.* [20-22] investigated Numerical simulation of natural convection of the nanofluid using a Buongiorno model. Malvandi and Ganji [23] studied Brownian motion and thermophoresis effects on slip flow of Alumina water nanofluid inside a circular microchannel in the presence of a magnetic. Kata *et al.* [24] discussed the effect of thermophoresis and Brownian

motion on the melting heat transfer of a Jeffrey fluid near a stagnation point towards a stretching surface using Buongiorno's model. Qasim *et al.* [25] studied heat and mass transfer in nanofluid thin film over an unsteady stretching sheet using Buongiorno's model. Pop *et al.* [26-27] studied free convection of a nanofluid in non-equilibrium porous cavity considering Buongiorno's model.

Noghrehabadi *et al.* [28] studied natural convection of nanofluid over vertical plate embedded in porous medium. Onsor Sayyar and Saghafian analyzed [29] numerical simulation of convective heat transfer of nonhomogeneous nanofluid using Buongiorno model. Saleh *et al.* [30] studied the natural convection of water-based copper and alumina nanofluids flow in a trapezoidal cavity. Their results showed that the effective heat transfer enhancement occurs for a trapezoidal cavity having an acute geometry inclined angle with a high concentration of copper nanoparticles. Soleimani *et al.* [31] studied natural convection heat transfer within a copper-water nanofluid filled a semi-annulus cavity. Their results showed that there is an optimum angle of turn for which the rate of heat transfer is the maximum for several thermal Rayleigh numbers. Sheremet *et al.* [32] discussed steady-state free convection in right-angle porous trapezoidal cavity filled by a nanofluid: Buongiorno's mathematical model. Garoosi *et al.* [33] investigate the numerical simulation of natural convection of the nanofluid in heat exchangers using a Buongiorno model. Al-Weheibi *et al.* [34] investigated numerical simulation of natural convection heat transfer in a trapezoidal enclosure filled with nanoparticles. Esfe *et al.* [35] studied natural convection in a trapezoidal enclosure filled with carbon nanotube and water-ethylene glycol nanofluid.

Alvario *et al.* [36] analyzed a numerical investigation of laminar flow of a water/ alumina nanofluid. Ramachandra and Suryanarayana [37] analyzed heat and mass transfer of Buongiorno's model nanofluid over linear and non-linear stretching surface with thermal radiation and chemical reaction. Khan *et al.* [38] studied numerical study of nanofluid flow and heat transfer over a rotating disk using Buongiorno's model. Demirdzic *et al.* [39] studied about the fluid flow and heat transfer test problems solutions for non- orthogonal grids: Bench mark. De Davis *et al.* [40] studied the natural convection in a square cavity: Venkatadri *et al.* [41] simulated the natural convection heat transfer in a 2D trapezoidal enclosure and found that the fluid flow within the enclosure is formed with different shapes for different values of Pr . The flow rate is increased by enhancing the Rayleigh number.

From the above literature review, it is observed that few researches have been done using Buongiorno's model [42] including the effect of Brownian motion and thermophoresis. In spite of these researches more investigations are still needed especially for Brownian motion and thermophoresis effect on flow, temperature and concentration fields due to their huge applications. The Buongiorno's model is able to consider the effect of nanoparticle volume fraction distribution. This model can also explore the heat transfer phenomena caused by Brownian motion and thermophoresis by using similarity transformations. Using this model, the governing equations can be reduced to a set of ordinary differential equations which are easy to solve more accurately. Thus, the numerical study of Brownian motion and thermophoresis on free convective water based nanofluid flow in a trapezoidal enclosure using Buongiorno's model will be conducted in this thesis.

1.3 Objectives

The aim of this research is to investigate the effects of Brownian motion and thermophoresis on free convection in a trapezoidal enclosure. The specific objectives are:

- i) To analyze the natural convection in a trapezoidal cavity having sinusoidal wall temperature using Buongiorno's mathematical model.
- ii) To find the effects of Brownian motion and thermophoresis on velocity, temperature, concentration distributions as well as heat and mass transfer rates.

The possible outcomes of this research result are as follows:

- ❖ The effect of Brownian motion and thermophoresis on the fluid flow, temperature, and concentration will be identified.
- ❖ The flow, heat and concentration controlling parameters for a specific heat and mass transfer application in a trapezium shaped cavity will be obtained.
- ❖ The research output can be applied in flow and heat transfer in solar ponds and air conditioning in room.

1.4 Scope of the Thesis

A brief description of the present numerical investigation of heat-mass transfer inside a trapezoidal enclosure using nanofluids has been presented in this thesis through four chapters as stated below:

Chapter 1 contains introduction with the aim and objectives of the present work. This chapter also includes a literature review of the past studies on heat transfer using nanofluid which is relevant to the present work. Objectives of the present study have also been incorporated in this chapter.

Chapter 2 presents a short introduction of numerical method. Then, the Finite Element Method and Galerkin's Technique have been discussed in this chapter detail. Physical model of Trapezoidal enclosure is described. Creation of geometry, meshing, implementation of physics, boundary conditions, mathematical formulation and numerical computation have been included in this chapter.

In Chapter 3, the effects of Buoyancy ratio, thermophoresis, Prandtl number, Brownian motion, Rayleigh number and Lewis number have been presented. Results have been shown in the form of isothermal lines, stream lines and iso-concentration lines to better understand the heat transfer mechanism through trapezoidal enclosure. In addition, the variation of the average Nusselt Number at the left and right inclined walls of the enclosure has been shown for above mentioned parameters.

Finally, in chapter 4, the concluding remarks of the whole research and the recommendations for the future investigations have been presented systematically.

Chapter 2: Numerical Study of Buongiorno's Nanofluid Model

2.1 Introduction

Numerical analysis is the study of algorithms that use numerical approximation (as opposed to symbolic manipulations) for the problems of mathematical analysis (as distinguished from discrete mathematics). Numerical analysis naturally finds application in all fields of engineering and the physical sciences, but in the 21st century also the life sciences, social sciences, medicine, business and even the arts have adopted the process of scientific computations.

Fluid flow, heat and mass transfer problems can be analyzed theoretically or experimentally. From an economic point of view, the experimental investigation of these problems did not attract much attention due to their insufficient flexibility and applications. However, often experimental investigations are necessary to validate the numerical method. Any change in geometry requires a separate experimental system setup and the boundary conditions of the systems for their investigation. The involvement of time is also a reason to make it appealing. On the other hand, theoretical analyzes can be performed through analytical methods or numerical methods. Analytical solution methods for solving practical problems are not very popular. Numerical methods are extremely powerful problem-solving tools capable of handling large systems of equations, complex geometry, etc., which are often impossible to solve analytically. General closed form solutions are very ideal cases and the results obtained for specific problems can usually be found with identical boundary conditions. Numerical methods are an easy way to find solutions to problems of practical interest because it reduces superior mathematics to basic arithmetic operations.

2.2 Finite Element Method

The finite element method (FEM) is a numerical method for solving problems of engineering and mathematical physics. Typical problem areas of interest include structural analysis, heat transfer,

fluid flow, mass transport, and electromagnetic potential. The analytical solution of these problems generally requires the solution to boundary value problems for partial differential equations. The finite element method formulation of the problem results in a system of algebraic equations. The method approximates the unknown function over the domain. To solve the problem, it subdivides a large system into smaller, simpler parts that are called finite elements. The simple equations that model these finite elements are then assembled into a larger system of equations that models the entire problem. FEM then uses variation methods from the calculus of variations to approximate a solution by minimizing an associated error function. Studying or analyzing a phenomenon with FEM is often referred to as finite element analysis (FEA).

A finite element method is characterized by a variation formulation, a discretization strategy, one or more solution algorithms and post-processing procedures. Examples of variation formulation are the Galerkin method, the discontinuous Galerkin method, mixed methods, etc. A discretization strategy is understood to mean a clearly defined set of procedures that cover (a) the creation of finite element meshes, (b) the definition of basis function on reference elements (also called shape functions) and (c) the mapping of reference elements onto the elements of the mesh. Examples of discretization strategies are the h-version, p-version, hp-version, x-FEM, isogeometric analysis, etc. Each discretization strategy has certain advantages and disadvantages. A reasonable criterion in selecting a discretization strategy is to realize nearly optimal performance for the broadest set of mathematical models in a particular model class. There are various numerical solution algorithms that can be classified into two broad categories; direct and iterative solvers. These algorithms are designed to exploit the sparsity of matrices that depend on the choices of variation formulation and discretization strategy.

Post processing procedures are designed for the extraction of the data of interest from a finite element solution. In order to meet the requirements of solution verification, postprocessors need to provide for a posteriori error estimation in terms of the quantities of interest. When the errors of approximation are larger than what is considered acceptable then the discretization has to be changed either by an automated adaptive process or by action of the analyst. There are some very efficient postprocessors that provide for the realization of super convergence.

2.3 Galerkin's Technique

In mathematics, in the area of numerical analysis (the study of algorithms that use numerical approximation), Galerkin's method is a class of methods for converting a continuous operator problem (such as a differential equation) to a discrete problem. In principle, it is the equivalent of applying the method of variation of parameters to a function space, by converting the equation to a weak formulation. Typically, one then applies some constraints on the function space to characterize the space with a finite set of basic functions. In applied mathematics, methods of weighted residuals are methods for solving differential equations. The solutions of these differential equations are assumed to be well approximated by a finite sum of test functions. In such cases, the selected method of weighted residuals is used to find the coefficient value of each corresponding test function. The resulting coefficients are made to minimize the error between the linear combination of test functions, and actual solution, in a chosen norm.

Suppose, a linear differential operator D acting on a function u to produce a function p , $D(u(x)) = p(x)$.

We wish to approximate u by a function \tilde{u} , which is a linear combination of basic functions chosen from a linearly independent set.

That is, $u \cong \tilde{u} = \sum_{i=1}^n a_i \phi_i$

Now, when substituted into the differential operator, D , the result of the operations is not, in general, $p(x)$.

Hence a error or residual will exist: $E(x) = R(x) = D(\tilde{u}(x)) - p(x) = 0$.

The notion in the method of weighted residual (MWR) is to force the residual to zero in some average sense over the domain.

A weighted residual is simply the integral over the domain of the residual multiplied by a weight function $\omega(x)$. A weighted residual is $\int_{\Omega} \omega(x) R(\tilde{T}, x) dx$

By choosing N weight functions, $\omega_i(x)$ for $i = 1, \dots, N$ and setting these N weighted residuals to zero, we obtain N equations which we solve to determine the N unknown values of α_j .

We define the weighted residual for $\omega_i(x)$ to be

$$R_i(\bar{T}) = \int_{\Omega} \omega_i(x) R(\bar{T}, x) dx$$

The method of weighted residuals requires

$$R_i(\bar{T}) = 0 \quad \text{for } i = 1, 2, \dots, N.$$

In the method of weighted residuals, the next step is to determine appropriate weight functions. A common approach, known as the Galerkin method, is to set the weight functions equal to the functions used to approximate the solution. That is,

$$\omega_i(x) = \phi_i(x) \text{ (Galerkin)}$$

As a special case of the Galerkin process, the FEM is often added. In mathematical terms, the procedure is to construct an integral of the residual and weight functions of the internal product and set the integral to zero.

2.4 Physical Model

The schematic diagram of the studied configuration has been depicted in the Figure 2.1. It consists of a two-dimensional trapezoidal enclosure of height 1.3 m. The length of top, bottom, and inclined walls are 1, 1.8 and 1.36 m, respectively. Top and bottom parallel surfaces have been kept as adiabatic. All the walls have been considered no slip and impermeable. The sinusoidal temperature and nanoparticles distributions have been imposed on the left and right inclined walls of the enclosure. The top and bottom walls are insulated walls. The inclination angle is 17.5 degree. The left and right walls make this angle with vertical lines according to clockwise and anticlockwise directions, respectively. The gravity acts in the vertical direction and there is no viscous dissipation. Thermophoresis and Brownian motion effects are included in our study in the absence of chemical reaction. The base fluid (water) and the solid nanoparticles are in thermal equilibrium. Buongiorno's approximation issued to determine the variation of density in the buoyancy term where the other thermo-physical properties of the nanofluid are assumed constant.

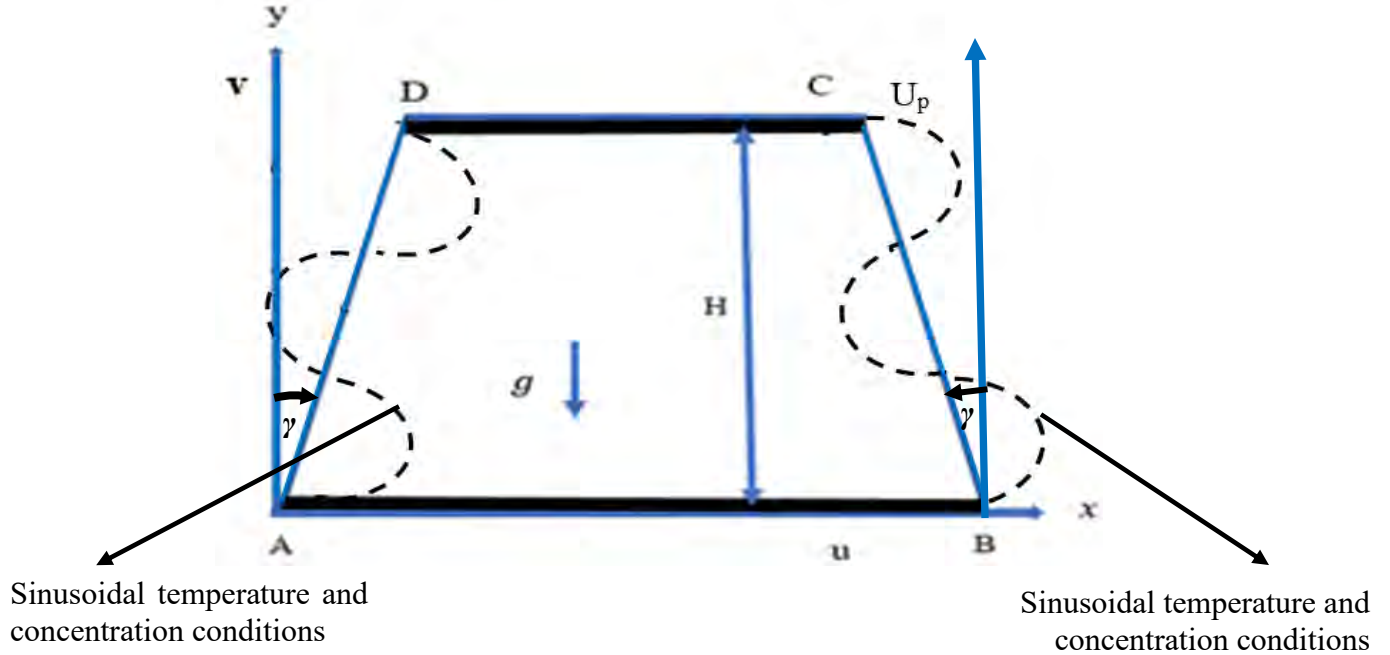


Figure 2.1: Physical model

2.5 Mathematical Model

The fluid domain inside the cavity has been considered as a continuum. The flow is assumed to be incompressible flow, no chemical reactions, negligible external forces, negligible viscous dissipation, negligible radiative heat transfer. The governing partial differential equations of the fluid (conservation of mass, momentum, energy and nanoparticles concentration) in dimensional form according to [1, 5, 43-46] have been given bellow:

Continuity equation:

$$\left(\frac{\partial u}{\partial x} + \frac{\partial v}{\partial y}\right) = 0 \quad (1)$$

x-momentum equation:

$$\rho_f \left(u \frac{\partial u}{\partial x} + v \frac{\partial u}{\partial y}\right) = -\frac{\partial P}{\partial x} + \mu_f \left(\frac{\partial^2 u}{\partial x^2} + \frac{\partial^2 u}{\partial y^2}\right) \quad (2)$$

y-momentum equation:

$$\rho_f \left(u \frac{\partial v}{\partial x} + v \frac{\partial v}{\partial y}\right) = -\frac{\partial P}{\partial y} + \mu_f \left(\frac{\partial^2 v}{\partial x^2} + \frac{\partial^2 v}{\partial y^2}\right) + \{C\rho_p + (1 - C)[(\rho_f(1 - \beta(T - T_c)))]\}g \quad (3)$$

Energy conservation equation:

$$u \frac{\partial T}{\partial x} + v \frac{\partial T}{\partial y} = \alpha_f \left(\frac{\partial^2 T}{\partial x^2} + \frac{\partial^2 T}{\partial y^2} \right) + D_B \left(\frac{\partial C}{\partial x} \frac{\partial T}{\partial x} + \frac{\partial C}{\partial y} \frac{\partial T}{\partial y} \right) + \left(\frac{D_T}{T_c} \right) \left[\left(\frac{\partial T}{\partial x} \right)^2 + \left(\frac{\partial T}{\partial y} \right)^2 \right] \quad (4)$$

Nanoparticle conservation equation:

$$u \frac{\partial C}{\partial x} + v \frac{\partial C}{\partial y} = D_B \left(\frac{\partial^2 C}{\partial x^2} + \frac{\partial^2 C}{\partial y^2} \right) + \frac{D_T}{T_c} \left(\frac{\partial^2 T}{\partial x^2} + \frac{\partial^2 T}{\partial y^2} \right) \quad (5)$$

Where u and v are the velocity components, p is the pressure, ρ is the density, ρ_f is the density of the nanofluid, μ is the dynamic viscosity, α is the thermal diffusivity, β is the thermal expansion, T is the temperature and C is the nanoparticle's concentration.

The following dimensional boundary conditions have been assigned:

On top wall: $u = v = 0, \frac{\partial T}{\partial y} = 0, \frac{\partial c}{\partial y} = 0$

On bottom wall: $u = v = 0, \frac{\partial T}{\partial y} = 0, \frac{\partial c}{\partial y} = 0$

On left inclined wall: $u = v = 0,$

$$T = T_c + (T_h - T_c) A \{ \sin(y - 0.3x) - x - 0.3y \};$$

$$C = C_c + (C_h - C_c) A \{ \sin(y - 0.3x) - x - 0.3y \}$$

On right inclined wall: $u = v = 0,$

$$T = T_c + (T_h - T_c) A \{ \sin(0.3x + y - 0.54) + 0.3y - x + 1.8 \}$$

$$C = C_c + (C_h - C_c) A \{ \sin(0.3x + y - 0.54) + 0.3y - x + 1.8 \}$$

Also, as the both inclined walls containing heating and cooling regions, we have to calculate the Nusselt number on both walls. The rate of heat transfer is computed at the left and right inclined walls and is expressed in terms of the local Nusselt number:

$$Nu = -\frac{hH}{k} = -\frac{\partial T}{\partial n} H$$

Where, h and n are the local convective heat transfer coefficient and dimensional distances either along x or y direction acting normal to the left and right inclined surfaces respectively.

The transformation of non-dimensional parameters has been defined as the following

$$\text{forms: } X = \frac{x}{H}, Y = \frac{y}{H}, U = \frac{uH}{\alpha}, V = \frac{vH}{\alpha}, P = \frac{uH^2}{\rho\alpha^2}, \theta = \frac{T-T_c}{T_h-T_c}, \varphi = \frac{C-C_c}{C_h-C_c} \quad (6)$$

Using these parameters, Equations (1) - (5) can be written in a non-dimensional form:

$$\frac{\partial U}{\partial X} + \frac{\partial V}{\partial Y} = 0, \quad (7)$$

$$U \frac{\partial U}{\partial X} + V \frac{\partial U}{\partial Y} = -\frac{\partial P}{\partial X} + Pr \left(\frac{\partial^2 U}{\partial X^2} + \frac{\partial^2 U}{\partial Y^2} \right) \quad (8)$$

$$U \frac{\partial U}{\partial X} + V \frac{\partial V}{\partial Y} = -\frac{\partial P}{\partial Y} + Pr \left(\frac{\partial^2 V}{\partial X^2} + \frac{\partial^2 V}{\partial Y^2} \right) - Ra Pr Nr (\varphi - 1) + Ra Pr \theta, \quad (9)$$

$$U \frac{\partial \theta}{\partial X} + V \frac{\partial \theta}{\partial Y} = \frac{\partial^2 \theta}{\partial X^2} + Nb \left(\frac{\partial \varphi}{\partial X} \frac{\partial \theta}{\partial X} + \frac{\partial \varphi}{\partial Y} \frac{\partial \theta}{\partial Y} \right) + Nt \left[\left(\frac{\partial \theta}{\partial X} \right)^2 + \left(\frac{\partial \theta}{\partial Y} \right)^2 \right] \quad (10)$$

$$U \frac{\partial \varphi}{\partial X} + V \frac{\partial \varphi}{\partial Y} = \frac{1}{Le} \left(\frac{\partial^2 \varphi}{\partial X^2} + \frac{\partial^2 \varphi}{\partial Y^2} \right) - \frac{Nt}{Nb Le} \left(\frac{\partial^2 \theta}{\partial X^2} + \frac{\partial^2 \theta}{\partial Y^2} \right) \quad (11)$$

And the non-dimensional boundary conditions are as follows:

On top wall: $U = V = 0, \frac{\partial \theta}{\partial Y} = 0, \frac{\partial \varphi}{\partial Y} = 0$

On bottom wall: $U = V = 0, \frac{\partial \theta}{\partial Y} = 0, \frac{\partial \varphi}{\partial Y} = 0$

On left inclined wall: $U = V = 0,$

$$\theta = \varepsilon \{ \sin(Y - 0.3X) - X - 0.3Y \},$$

$$\varphi = \varepsilon \{ \sin(Y - 0.3X) - X - 0.3Y \}$$

On right inclined wall: $U = V = 0,$

$$\theta = \varepsilon \{ \sin(0.3X + Y - 0.54) - X + 0.3Y + 1.8 \},$$

$$\varphi = \varepsilon \{ \sin(0.3X + Y - 0.54) - X + 0.3Y + 1.8 \}$$

Here $Pr = \frac{v_f}{\alpha_f}$, $Le = \frac{\alpha_f}{D_B}$, $Nt = \frac{D_T(\rho C)_p(\theta_h - \theta_c)}{T_c(\rho C)_f \alpha_f}$, $Nb = D_B \frac{(\rho C)_p(\varphi_h - \varphi_c)}{(\rho C)_f \alpha_f}$,

$Nr = \frac{(\varphi_h - \varphi_c)(\rho_p - \rho_f)}{(1 - \varphi_c)\rho_f(\theta_h - \theta_c)}$ and $Ra = \frac{g\beta(\theta_h - \theta_c)(1 - \varphi_c)H^3}{v_f^2}$ be the Prandtl number, Lewis

number, thermophoresis, Brownian motion, buoyancy ratio and Rayleigh number, respectively.

The non-dimensional local Nusselt number at the inclined surfaces is $\overline{Nu} = -\frac{\partial \theta}{\partial N} N$

The normal temperature gradient can be written as $\frac{\partial \theta}{\partial N} = \frac{1}{N} \sqrt{\left(\frac{\partial \theta}{\partial X}\right)^2 + \left(\frac{\partial \theta}{\partial Y}\right)^2}$.

The average Nusselt number (Nu) is obtained by integrating the local Nusselt number along the

inclined surfaces and is defined by $Nu = -\frac{1}{N} \int_0^N \overline{Nu} dN$.

2.6 Computational Procedure

Using the Galerkin's weighted residual finite element technique [47-48] the momentum and energy balance equations have been solved using COMSOL Multiphysics. In this method, the solution domain has been discretized into finite element meshes, which have been composed of non-uniform triangular elements. Then the nonlinear and non-dimensional governing partial differential equations have been transferred into a system of integral equations by applying Galerkin weighted residual method. The basic unknowns for the governing partial differential equations (7-11) are the velocity components U , V , the temperature θ , concentration, φ and the pressure P . The six nodes with triangular element have been used in this numerical research. All six nodes have been associated with velocities as well as temperature while three corner nodes with pressure. The nonlinear algebraic equations so obtained have been modified by imposition of boundary conditions. These modified nonlinear equations have been transferred into linear algebraic equations by using Newton's method. Finally, these linear equations have been solved by using triangular factorization method. The convergence criterion for the solution procedure has been defined as $|\psi^{n+1} - \psi^n| \leq 10^{-6}$, where n is the number of iteration and ψ is a function of U , V , θ and φ .

2.6.1 Code validation

In order to authenticate the exactness of present numerical technique, the obtained graphical representation of streamlines and isothermal lines using the present numerical code have been compared with the results obtained by Venkatadri *et al.* [41].

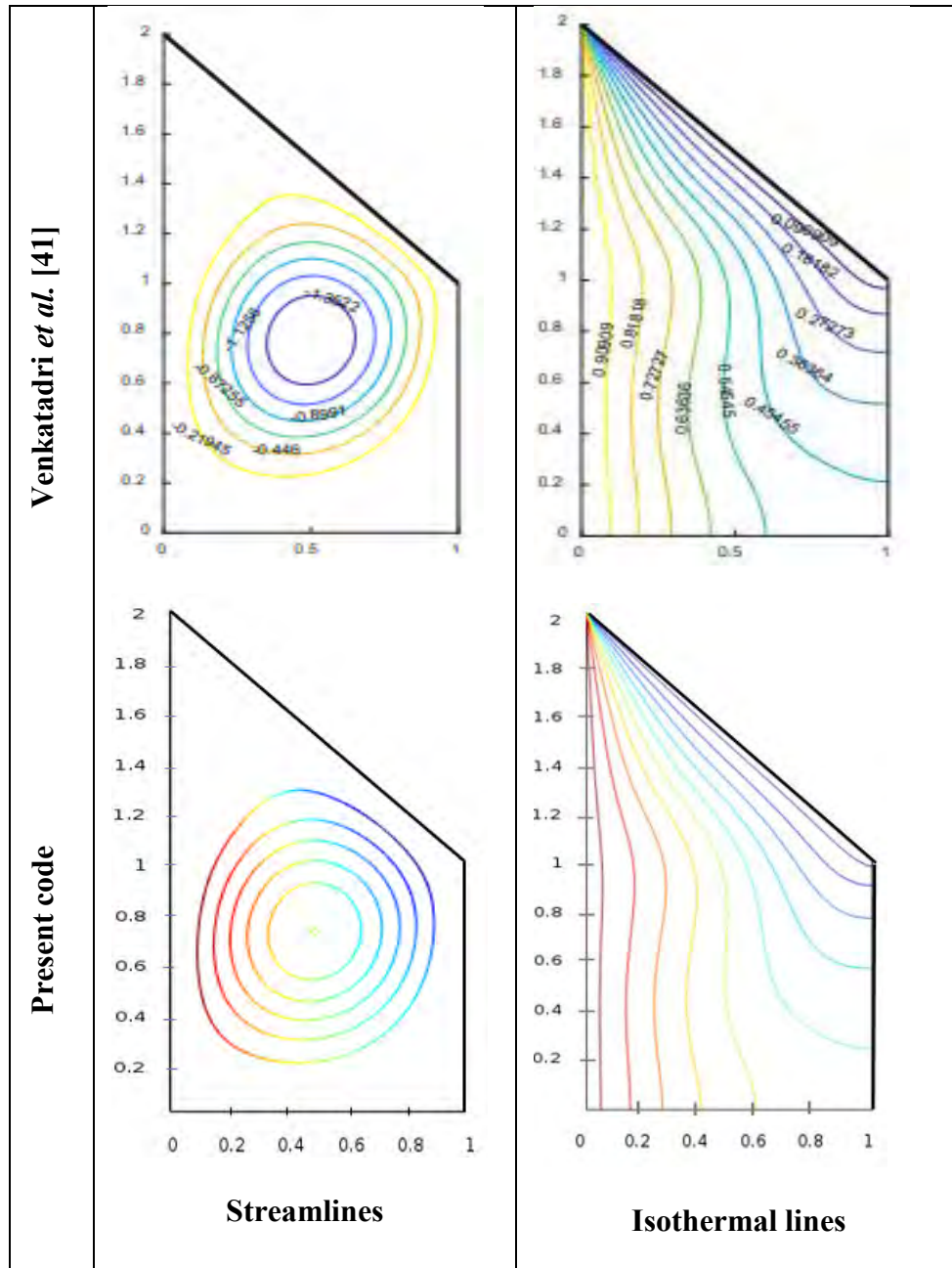


Figure 2.2: Code validation of the streamlines and isotherms between Venkatadri *et al.* [41] and that of present research at $Ra = 10^3$ and $Pr = 0.025$

They simulated numerically free convective heat transfer 2D model of trapezoidal cavity. These comparisons have been presented obviously in the figure 2.2. The code validation has been conducted while employing the dimensionless parameters as $Ra = 10^3$ and $Pr = 0.025$. A very good agreement has been found between the present numerical code results and the results of Venkatadri *et al.* [41]. These flattering comparisons provide confidence in the numerical results to be reported subsequently.

2.6.2 Mesh generation

The discrete locations at which the variables are to be calculated are defined by a mesh which covers the geometric domain on which the problem is to be solved. It divides the solution domain into a finite number of sub-domains called finite elements. The computational domains with irregular geometries by a collection of finite elements make the method a valuable practical tool for the solution of boundary value problems arising in various fields of engineering. Figure 2.3 displays the finite element mesh of the present physical domain. The meshing consists of triangular element with six nodes in boundaries.

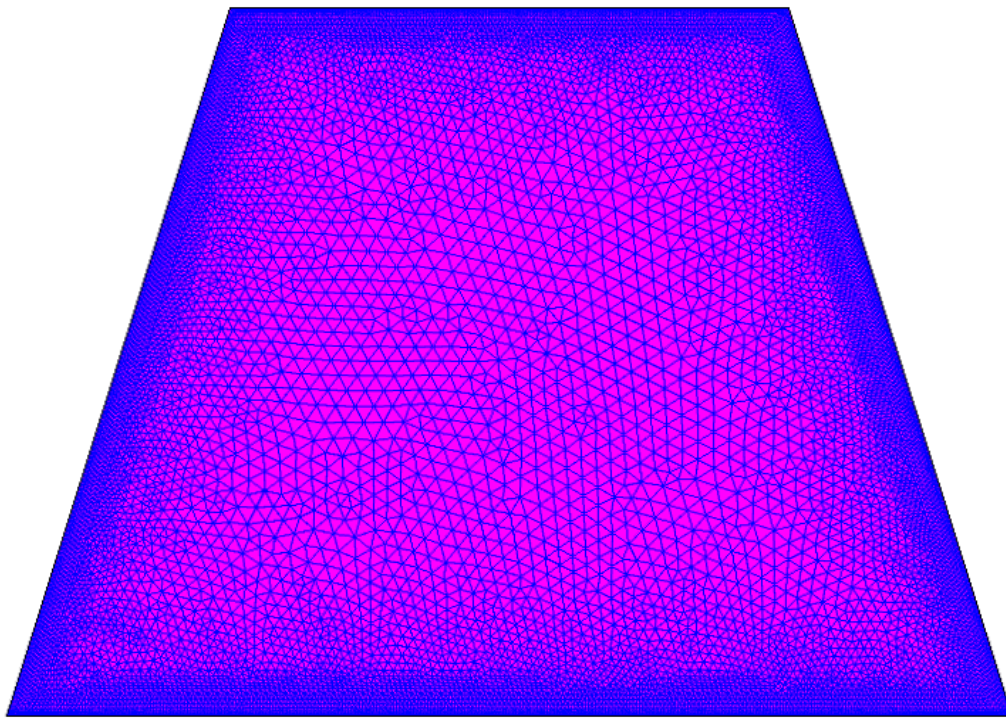


Figure 2.3: Mesh generation of the trapezoidal enclosure

2.6.3 Grid sensitivity test

In order to determine the proper grid size for this study, a grid independence test is conducted with five types of mesh for $Pr = 7$, $Ra = 10^4$, $Nt = Nr = Nb = 0.1$ and $Le = 10$ which has been shown in Table 2.1. Corresponding grid densities are 4925 nodes, 1602 elements, time 52 s; 7930 nodes, 2708 elements, 95s; 20320 nodes, 2708 elements, 112s; 49780 nodes, 18008 elements, 276s; and 75500 nodes, 28296 elements, 403s. The extreme value of Nu is used as the monitoring variable for sensitivity measure of the accuracy of the solution. Taking into account both the precision of numerical values and computational time, the present calculations are performed with 18082 nodes and 4484 elements grid system. Table 2.1, one can observe that no further improvement in accuracy occur using higher number of elements.

Table 2.1: Grid sensitivity check at $Pr = 7$, $Ra = 10^4$, $Nt = Nr = Nb = 0.1$ and $Le = 10$

Mesh type	Normal	Fine	Finer	Extra Fine	Extremely Fine
Elements	1602	2708	7142	18008	28296
Nu	0.243	0.564	0.774	0.985	0.9854
Time (s)	52	95	112	276	403

Chapter 3: Results and Discussions

3.1 Introduction

Free convection of heat transfer in a trapezoidal enclosure with sinusoidal temperature distributions on both side walls is examined numerically using Buongiorno's model. The numerical calculation is carried out for various values of Brownian motion (Nb) from 0.1 to 2, Prandtl number (Pr) from 0.7 to 10, Rayleigh number (Ra) from 10^2 to 10^5 , thermophoresis parameter (Nt) from 0.1 to 1.5, Lewis number (Le) from 1 to 10 and buoyancy ratio (Nr) from 0.1 to 0.7. These relevant parameters have a direct effect on the flow, thermal and concentration fields inside the considered cavity. The numerical results have been offered in terms of streamlines, isothermal lines, nanoparticle volume fraction contours and average Nusselt number (Nu) on both left and right inclined walls. In order to display the results out of these six independent parameters, five parameters have been kept as fixed (unless where stated) while the remainder single one has been varied as gathered in the following categories:

3.2 Effect of Lewis number

Figure 3.1 (a-c) illustrate the effect of Lewis number on streamlines, isothermal lines and iso-concentration lines in the range ($Le = 1 - 10$). For this effect the values of another parameter have been kept as fixed at $Pr = 7$, $Ra = 10^4$, $Nt = Nr = Nb = 0.1$. Blue color indicates the lowest value and red color represents the highest value in the streamlines, isothermal lines and iso-concentration lines. It is noticed from this figure that an increase of Lewis number leads to both significant changes in conservation of velocity, temperature and nanofluid concentration fields. Regardless of the Lewis number the convective cells are formed inside the cavity. The cells at the middle part vortices anti-clockwise direction whereas the cells at top and bottom are vortices clockwise direction inside the cavity of the figure 3.1(a). The main reason for an appearance of these circulations is an effect of inclined wall with sinusoidal temperature distribution. The vortices are separated by virtual horizontal and inclined wall which are both impervious and adiabatic. Convective cells are close to the vertical wall due to the large temperature difference in this zone. It should be noted that an intensity of cells in the middle part of the cavity is greater than an intensity of convective cells in the top and bottom part of the cavity.

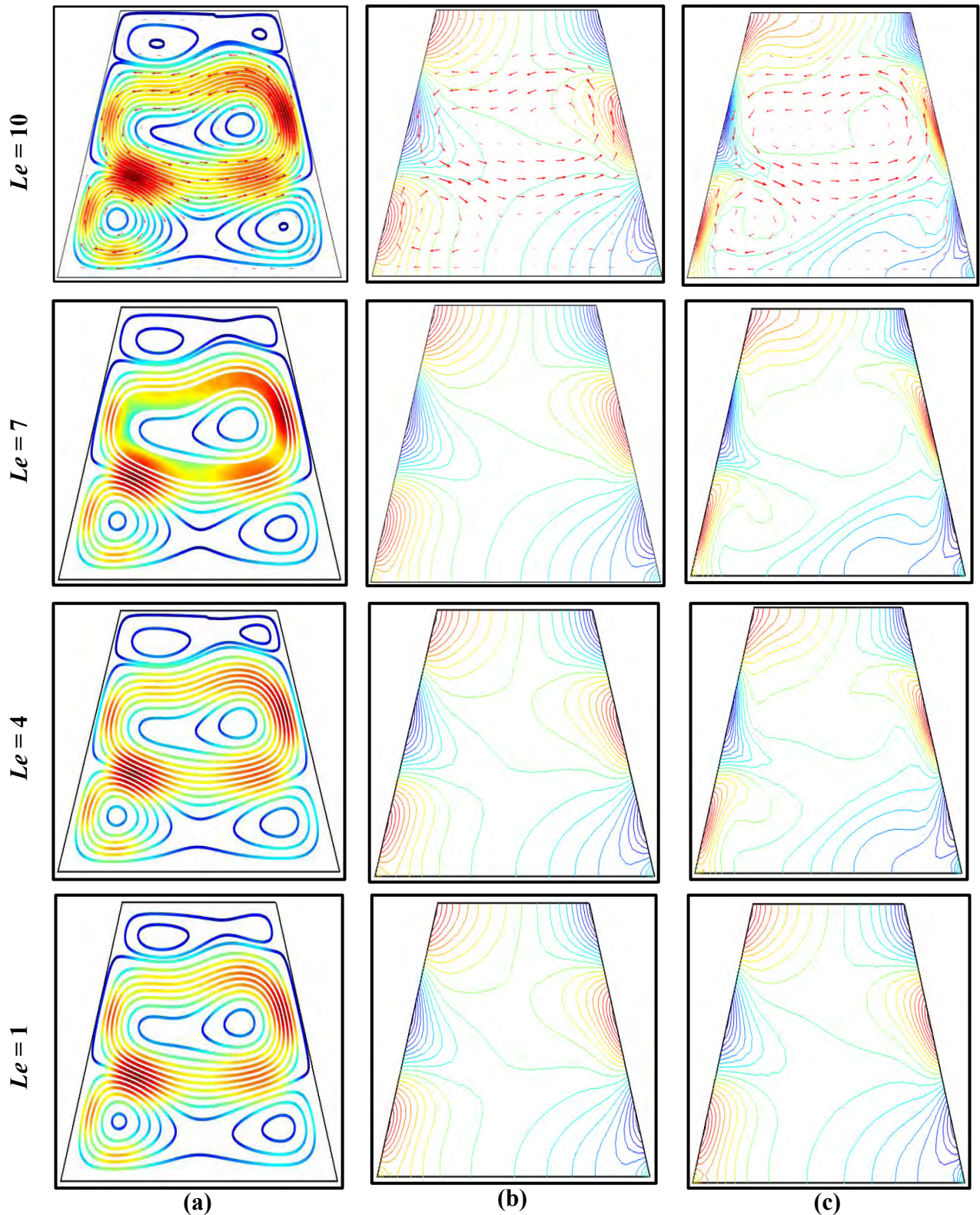


Figure 3.1: Effect of Lewis number on (a) streamlines, (b) isothermal lines and (c) iso-concentration at $Pr = 7$, $Ra = 10^4$, $Nt = Nr = Nb = 0.1$

It is seen from the figure 3.1(b) those convective cells cores are close to the vertical walls due to large temperature differences in these zones. An increase in the Lewis number does not change in all local fields of temperature inside the cavity. It physically means that flow with

large Lewis number prevent spreading nanoparticles in the nanofluid. Therefore, we have large homogeneous areas in the domain nonconsecutive cells. Only non-homogeneous area become more confined at $Le = 7$.

At $Le \leq 10$ the distribution of nano particle is non-homogeneous. It physically means that leads to spreading nanoparticle in the nanofluid. Therefore, we have the large non-homogeneous are in the domain of convective cells. Figure 3.1(c) shows the main variations with the Lewis number related to the iso-concentrations. These fields characterize the distributions of the nanoparticles volume fraction inside the trapezoidal cavity. Regardless of the Lewis number value, the intensity of non-convective cells close to the inclined wall is greater than the intensity of the central part of the cavity. The distribution is considered as non-homogeneous.

An effect of the dimensionless Lewis number on the average Nusselt number at left and right inclined walls is presented in the figure: 3.2. From figure it is noticed that an increase in Le from 1 to 10 leads to a significant increase in average Nusselt number at left and right vertical wall. The increasing rate of average Nusselt number at right and left wall are 0.7108% and 0.7081%. The increasing rate in average Nusselt number due to Lewis number at right wall is greater than the right wall. The increasing rate is 0.3813% higher for right wall than the left wall.

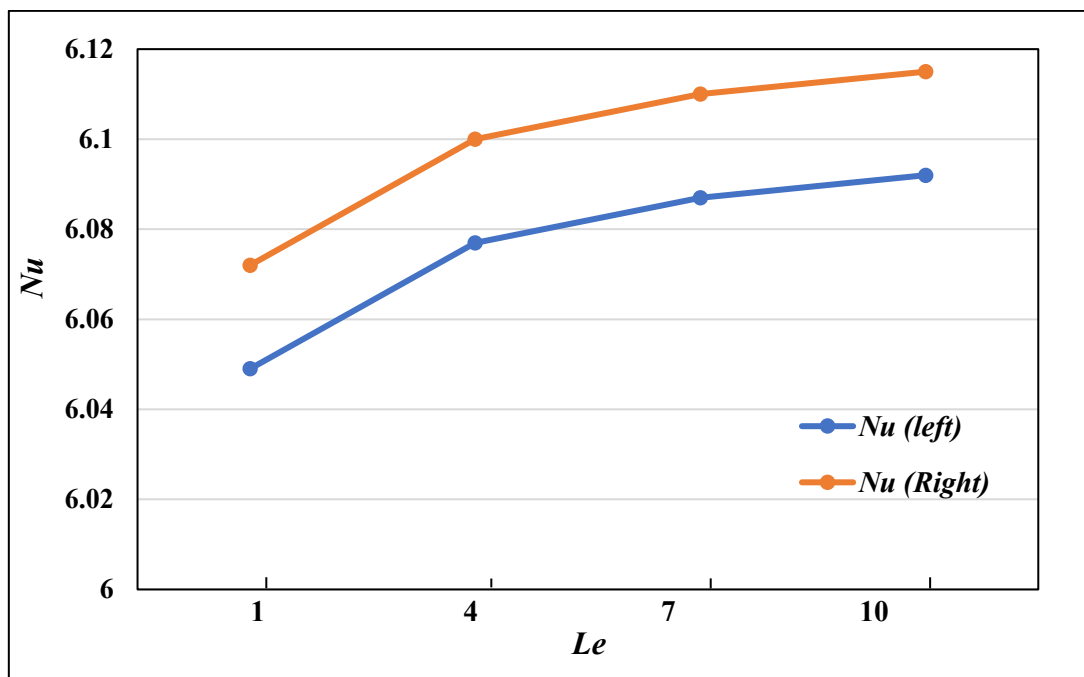


Figure 3.2: Average Nusselt number at left and right walls against Lewis number at $Pr = 7$, $Ra = 10^4$, $Nt = Nr = Nb = 0.1$

3.3 Effect of Thermophoresis

Figures 3.3 (a-c) illustrate the effect of thermophoresis parameter (Nt) from 0.1 to 1.5 on the velocity, temperature and nanoparticle concentration contours with fixed $Le = 10$, $Pr = 7$, $Ra = 10^4$, $Nr = Nb = 0.1$. Regardless of the thermophoresis parameter four non-convective cells are formed in the streamlines along the clockwise direction inside the cavity of the. An increase in Nt leads to changes in all characteristics (streamlines, isotherms, and iso-concentrations) that can be described in the following way. Regardless of the thermophoresis there is a small significant change in streamlines.

From the figure one can find the intensification and increase in size at the bottom part and attenuation and decrease in size at upper part of the cavity. It can be seen that the shape of the primary cells at middle side has been changed a little bit due to increase in Nt . It is important to notice that there is a significant change in oval shape at the top side. The oval shape core at the top has been smaller than the before shape. At the same time, it is observed from the figure 3.3 (b) that an increase in thermophoresis parameter leads to more intensive heating of the bottom part than the upper part of the enclosure. Such changes characterize decrease in temperature differences in the bottom part and increase in temperature difference at upper part.

It should be noted from the figure 3.3 (c) that the main variations with the thermophoresis parameter are related to the iso-concentrations. An increase in Nt leads to essential changes of the nanoparticles volume fraction both in the upper and bottom parts of the cavity. In general, these distributions can be considered as non-homogeneous.

An effect of the dimensionless time and thermophoresis parameter on the average Nusselt number at left and right vertical wall is depicted in Fig. 3.4 It is necessary to note that an increase in Nt leads to an increase in the average Nusselt number. From the figure it is noticed that the increase in the average Nusselt number at the right wall is 36.37% and at left wall is 35.49% for $Nt = 0.1$ to $Nt = 1.5$. The increase in the average Nusselt number at the right wall is higher compared with the left wall and the increasing rate at right wall is 2.479% compared with the left wall.

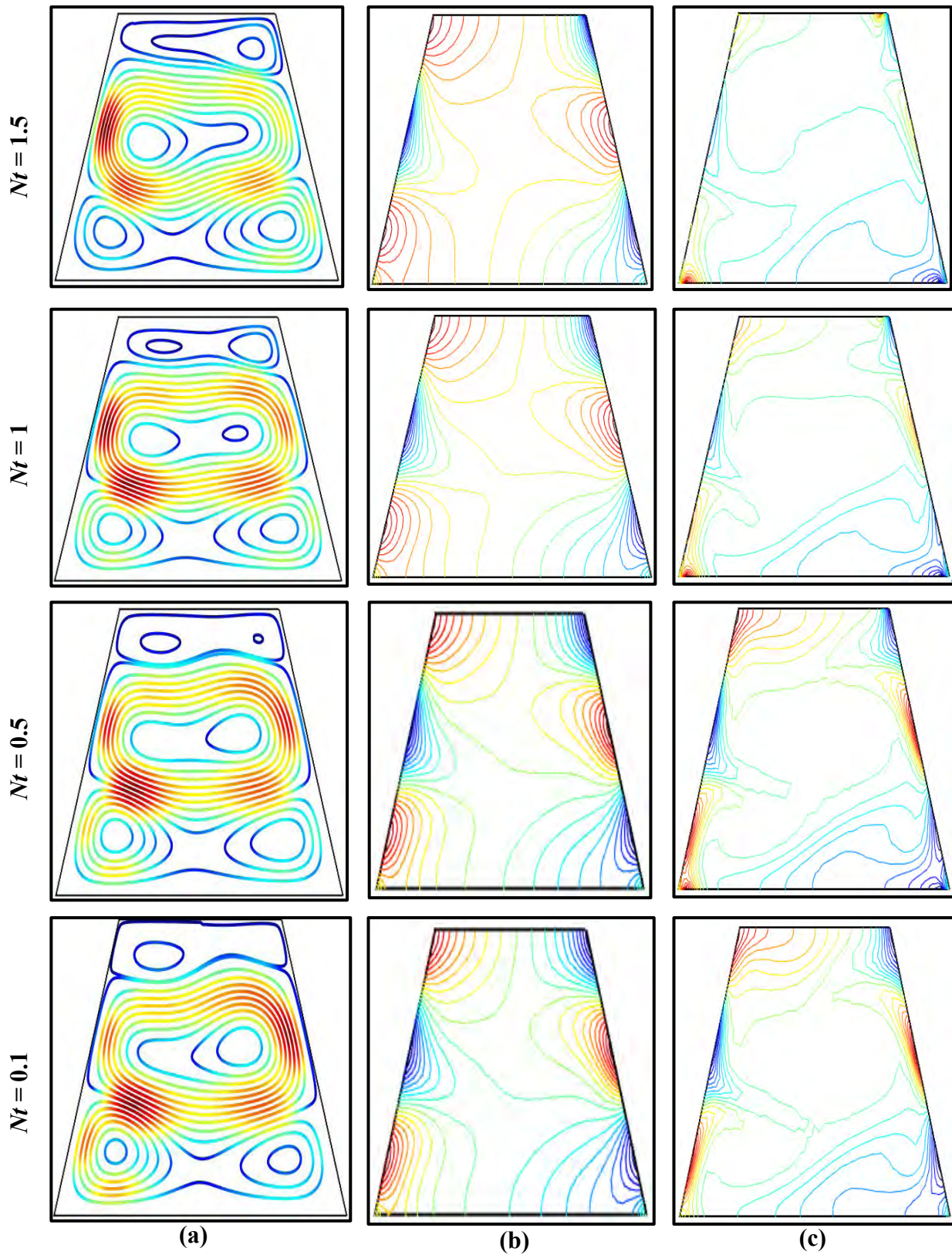


Figure 3.3: Effect of thermophoresis parameter on (a) streamlines, (b) isothermal lines and (c) iso-concentration lines at $Le = 10$, $Pr = 7$, $Ra = 10^4$, $Nr = Nb = 0.1$

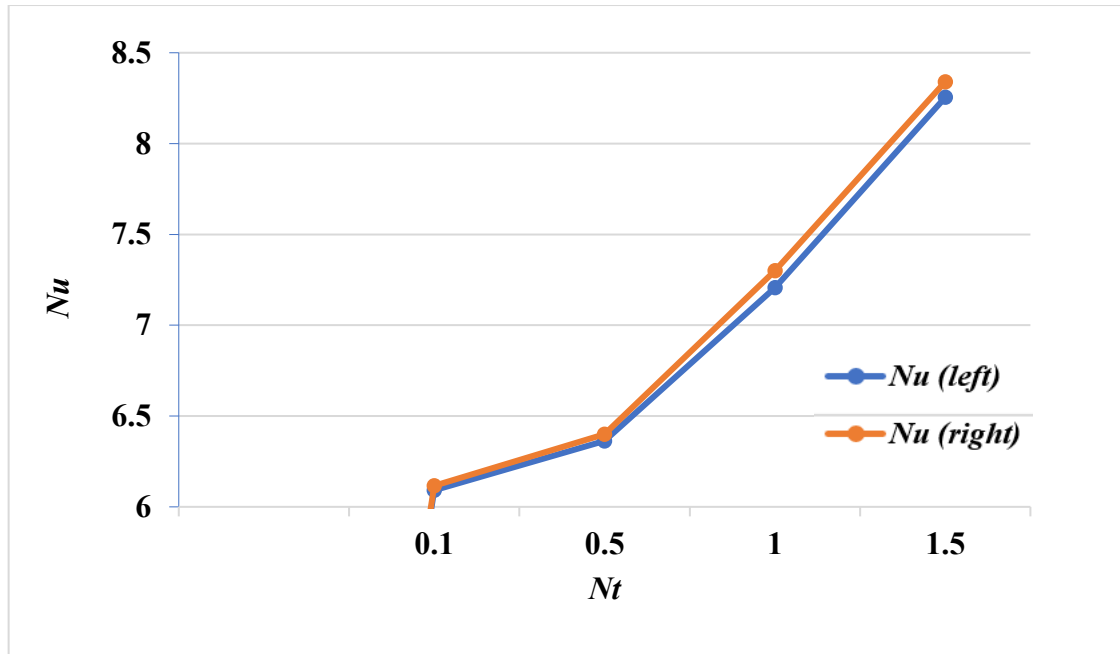


Figure 3.4: Average Nusselt number at left and right wall against thermophoresis parameter at $Le = 10$, $Pr = 7$, $Ra = 10^4$, $Nr = Nb = 0.1$

3.4 Effect of Prandtl Number

Figure 3.5(a-c) displays the effect of Prandtl number from 0.7 to 10 on velocity, temperature and concentration contours with fixed $Ra = 10^4$, $Nt = Nr = Nb = 0.1$ and $Le = 10$. From the streamlines contours it is found that there is a small change in non-convective cell. For $Pr = 0.7$ it is noticed that the primary elliptic circulation cells and small oval shape core has been created. At $Pr = 4$ it can be seen that shape of the primary cell remains same but the oval shape at top side has been changed a little bit and it is important to notice that oval shape core at the top has been less than the before shape. On the other hand, when $Pr = 7$ and $Pr = 10$, there is little distinction in the streamlines that gradually increment of oval shape core. There is little change in isotherm.

One important thing is noticed from the figure 3.5(b) that an increase in Prandtl number (Pr) leads increase in intensity of the non-convective cell inside the cavity. The intensity is higher at bottom and upper part for the left wall whereas the intensity is higher at middle part for the right wall.

Figure 3.5(c) that the main variations with the Prandtl number (Pr) are related to the iso-concentrations. An increase in Pr leads to essential changes of the nanoparticles volume fraction both in the upper and bottom parts of the cavity and these distributions can be considered as non-homogeneous.

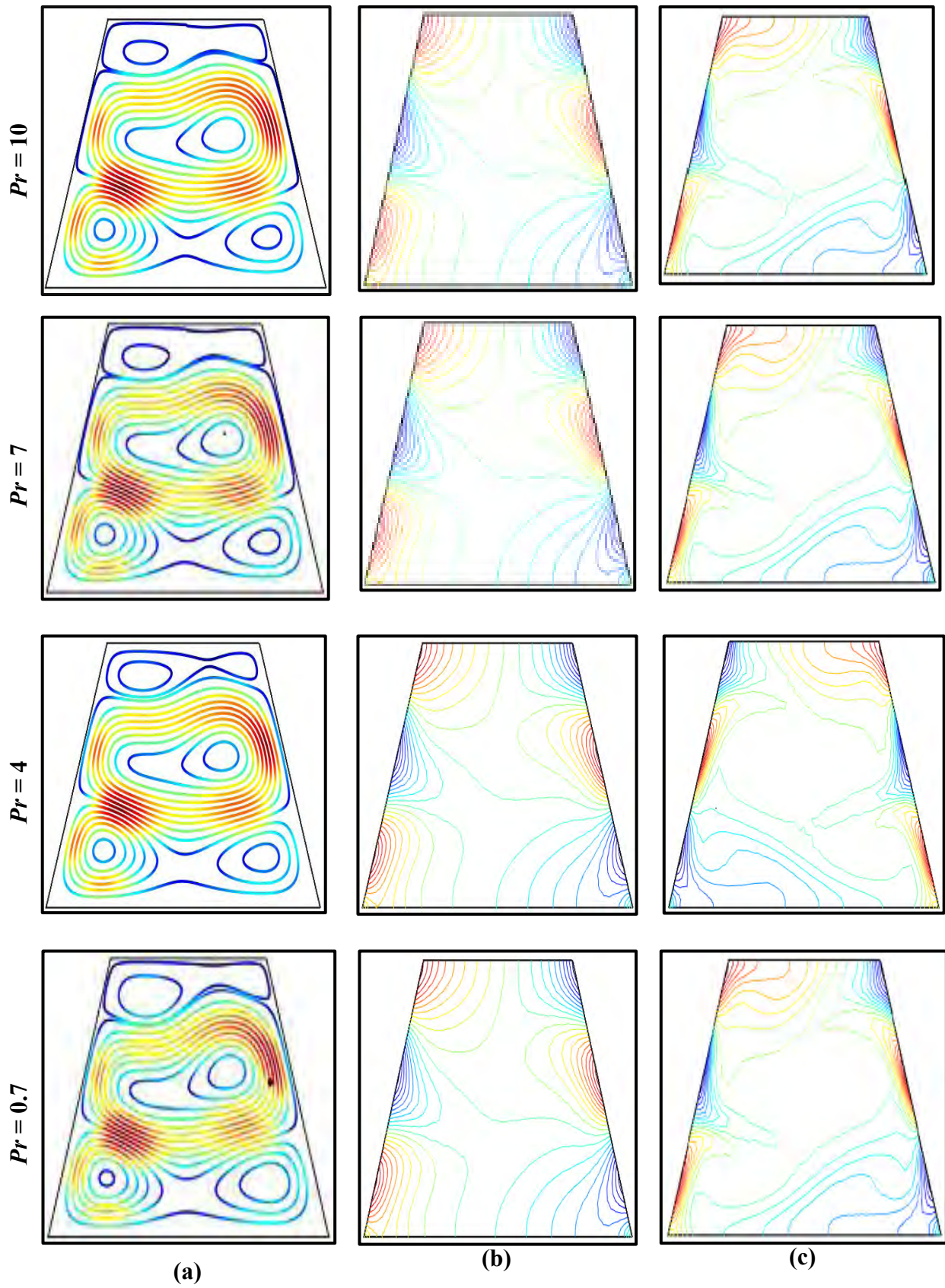


Figure 3.5: Effect of Prandtl number on (a) streamlines, (b) isothermal lines and (c) iso-concentration lines at $Ra = 10^4$, $Nt = Nr = Nb = 0.1$ and $Le = 10$

An effect of the Prandtl number (Pr) on the average Nusselt number at left and right inclined walls is presented in the figure 3.6. An increase in Prandtl number from 0.7 - 4 leads to highly increase in average Nusselt number but from 4-10 leads to a small amount of increase in average Nusselt number. The average increase in Nusselt number due to Prandtl number at left wall is 0.4104% and right wall 0.893%. From this calculation we see that average increase in Nusselt number due to Prandtl number at right inclined wall is greater than left inclined wall.

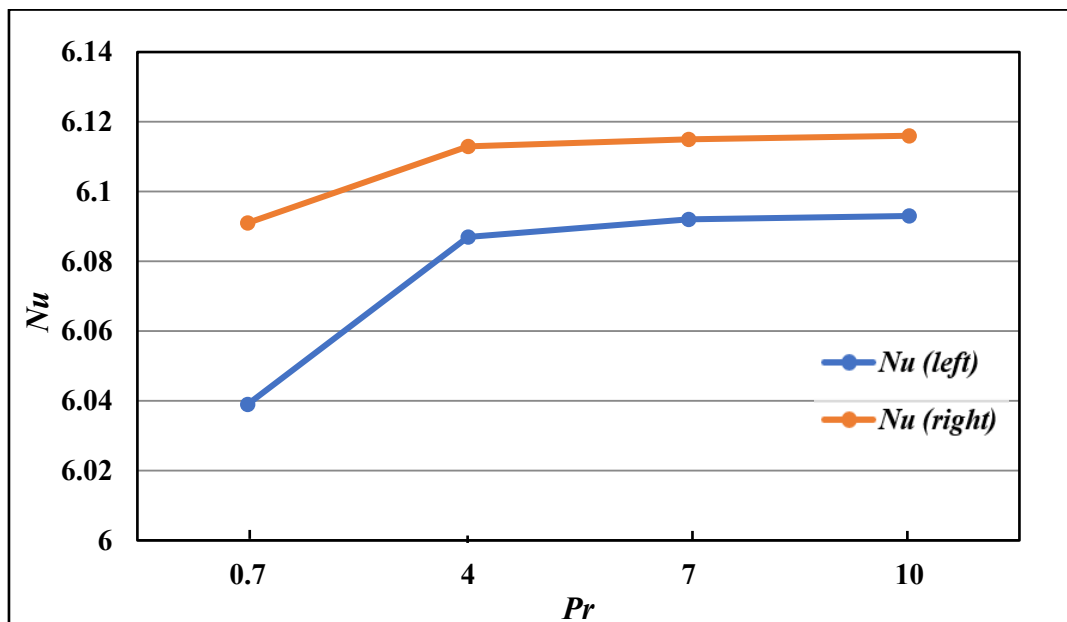


Figure 3.6: Average Nusselt Number at the left and right walls against Prandtl number at $Le = 10$, $Ra = 10^4$, $Nt = Nr = Nb = 0.1$

3.5 Brownian Motion Effect

Figure 3.7 (a-c) illustrate the effect of Brownian motion on streamlines, isothermal lines and iso-concentration lines in the range ($Nb = 0.1-2.0$). For this effect the values of another parameter have been kept as fixed at $Pr = 7$, $Ra = 10^4$, $Nt = Nr = 0.1$ and $Le = 10$. It is noticed from this figure that an increase of Brownian motion parameter leads to both significant changes in conservation of velocity, temperature and nanofluid concentration fields. Regardless of the Brownian motion the non-convective cells are formed in the streamlines along the anti-clockwise direction inside the cavity of the figure 3.7(a). The main reason for an appearance of these circulations is an effect of the sinusoidal temperature distribution at inclined walls of the cavity. The vortices are separated by virtual horizontal and inclined wall which are both impervious and adiabatic. Non-convective cells are close to the inclined wall due to the large temperature difference in this zone. An increase of

Brownian motion parameter there is a small change in intensity and configuration in the cells and isotherm.

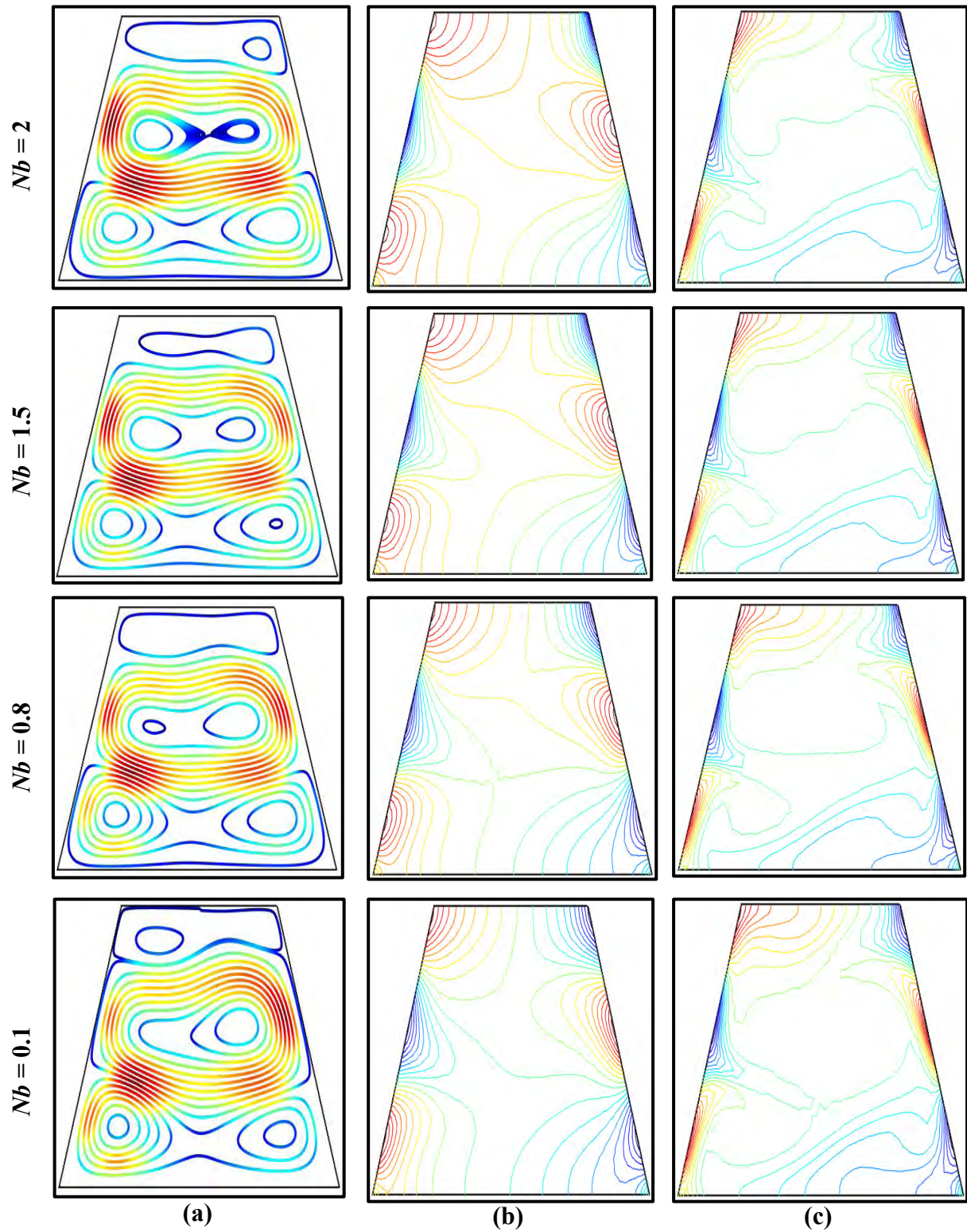


Figure 3.7: Effect of Brownian motion on (a) streamlines, (b) isothermal lines and (c) iso-concentration at $Pr = 7$, $Ra = 10^4$, $Nt = Nr = 0.1$ and $Le = 10$.

According to figure 3.7(b) it is possible to conclude that an increment in Nb leads to homogeneity of distribution inside the cavity. It also be noticed that the temperature variation is increased both in the top and bottom part with the increase Brownian motion parameter

A significant variation in iso-concentration with the Brownian motion parameter is found in the figure 3.7 (c). An increase in Nb leads to essential changes of the nanoparticles volume fraction both in the upper and bottom parts of the cavity and these distributions can be considered as non-homogeneous.

An effect of the Brownian motion parameter (Nb) on the average Nusselt number at left and right inclined walls is presented in the figure 3.8. An increase in Nb from 0.1 to 2 leads to an increase in average Nusselt number on both left and right wall. The average increase in Nusselt number due to Nb parameter at right wall is greater than the left wall. The increasing rate of average Nusselt number is approximately 34.75% and 34.27% for the right and left walls, respectively for rising values of Brownian motion. After calculation it is found that the average Nusselt number 1.40% higher for right wall compared with left wall.

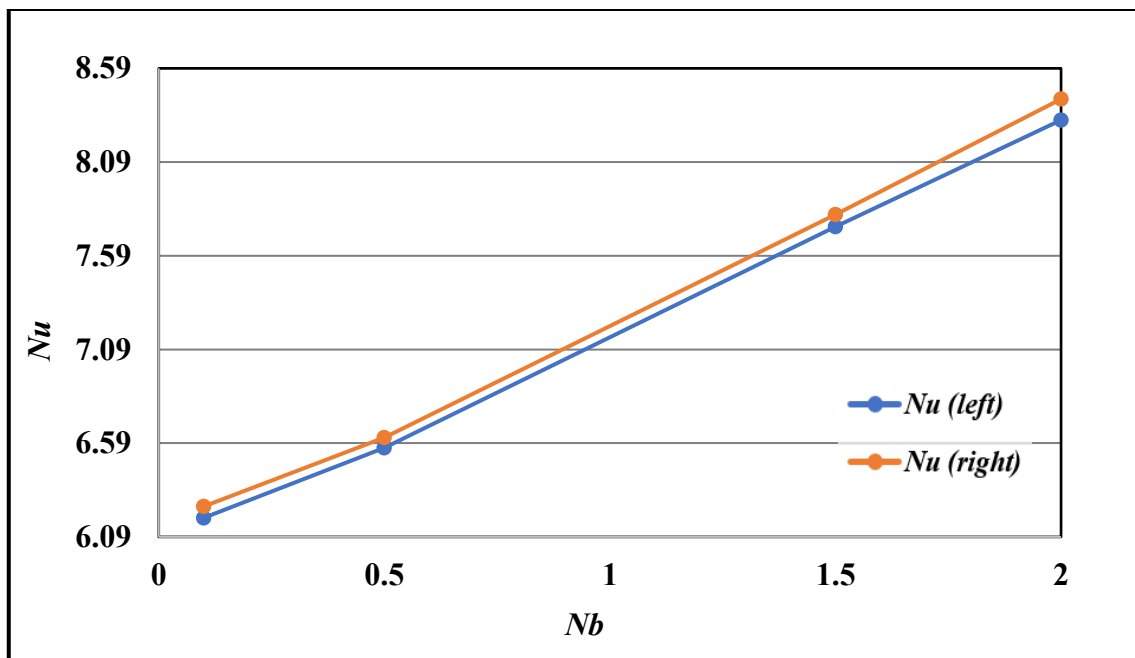


Figure 3.8: Average Nusselt Number at the left and right walls against the Brownian motion effect at $Pr = 7$, $Ra = 10^4$, $Nt = Nr = 0.1$, $Le = 10$

3.6 Effect of Buoyancy Ratio

Figure 3.9(a-c) illustrate the effect of buoyancy ratio on streamlines, isothermal lines and iso-concentration lines in the range ($Nr = 0.1- 0.7$). For this effect the values of another parameter have been kept as fixed at $Pr = 7$, $Ra = 10^4$, $Nt = Nr = 0.1$ and $Le = 10$.

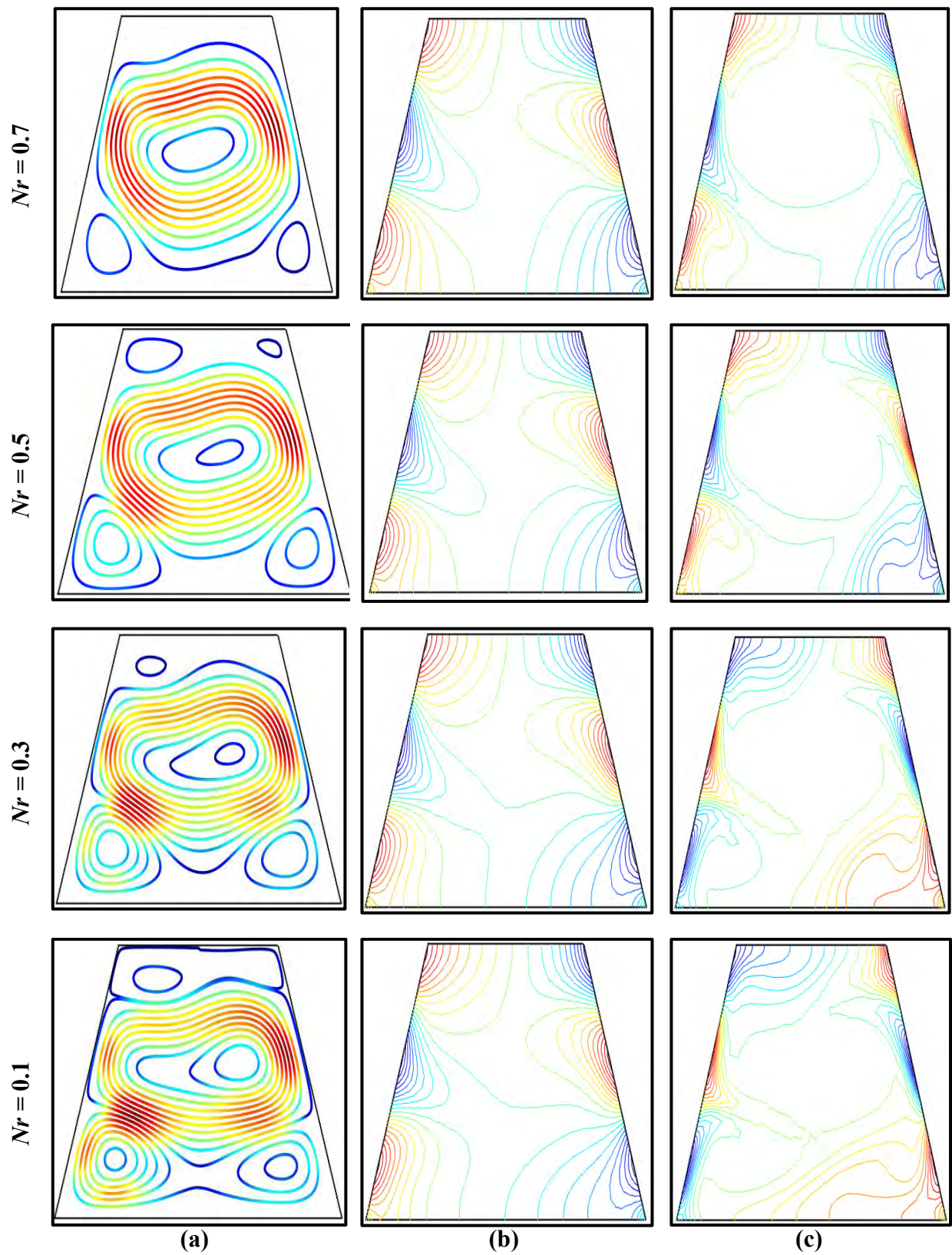


Figure 3.9: Effect of buoyancy ratio on (a) streamlines, (b) isothermal lines and (c) iso-concentration lines at $Pr = 7$, $Ra = 10^4$, $Nt = Nb = 0.1$ and $Le = 10$.

It is noticed from this figure that an increase of buoyancy ratio leads to both significant changes in conservation of velocity, temperature and nanofluid concentration fields. Regardless of the buoyancy ratio the non-convective cells are formed in the streamlines along the anti-clockwise direction inside the cavity of the figure 3.9(a). There is significant change on both the primary and oval shape. The primary shape at $Nr = 0.3$ is bent through a little bit than the previous cells. Finally, the cells turned into circular shape. The oval contour shape at top and bottom part of the cavity gradually decreases with the increase in buoyancy ratio.

Non-convective cells are close to the inclined wall due to the large temperature difference in this zone of the figure 3.9(b). An increase of buoyancy ratio parameter there is a small change in intensity and configuration in the isotherm. The enrichment of the thermal conductivity produces denser isotherms which is the indication of transfer of temperature. From the figure 3.9(b), it is evident that with the increase of the value of Nr heat transfer rate increases.

With the increase in Nr iso-concentration lines characterize a decrease in nanoparticle volume fraction in the upper part and increase in the bottom part of the figure 3.9 (c). Cells are close to the inclined wall due to the large temperature difference which refers the intensification in this zone.

An effect of the buoyancy ratio (Nr) on the average Nusselt number at left and right inclined walls is presented in the figure 3.10. An increase in Nr from 0.1- 0.7 leads to significant decrease in average Nusselt number. The average decrease in Nusselt number due to Nr at right wall is greater than the left wall. The decreasing rates of left and right wall are 1.101% and 1.104%, respectively. Decreasing rate at right wall compared with left wall is 0.272%.

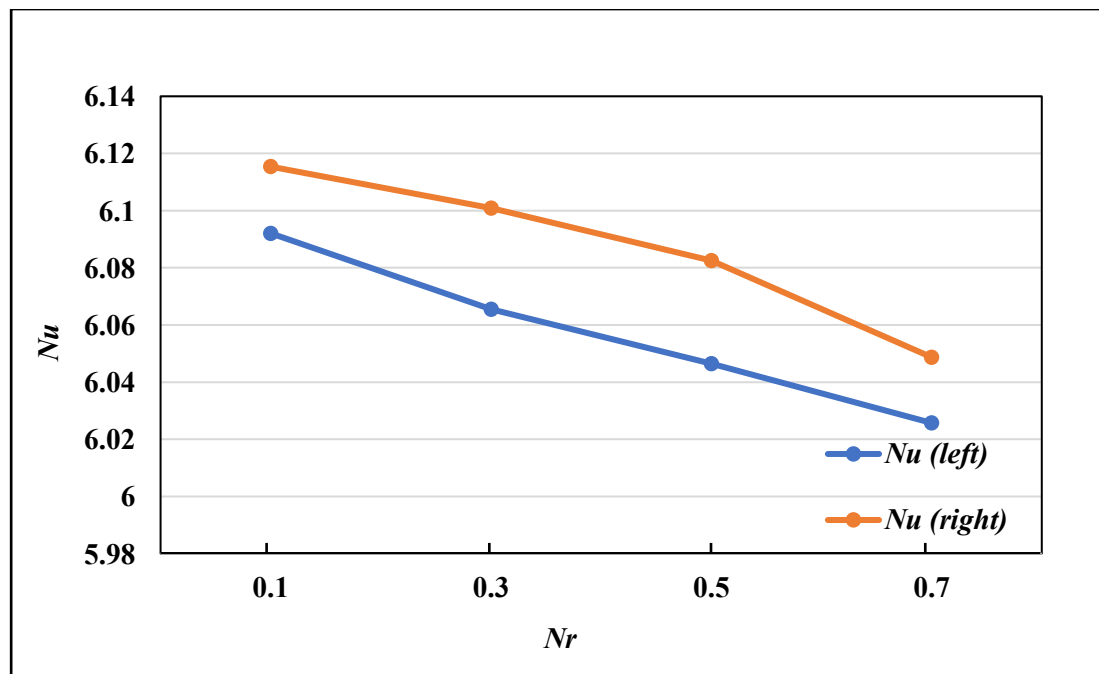


Figure 3.10: Average Nusselt Number at the left and right walls against buoyancy ratio at $Le = 10$, $Ra = 10^4$, $Pr = 7$ and $Nt = Nb = 0.1$

3.7 Effect of Rayleigh number

Figure 3.11(a-c) illustrate the effect of Rayleigh number on streamlines, isothermal lines and iso-concentration lines in the range ($Ra = 10^2$ - 10^5) For this effect the values of another parameter have been kept as fixed at $Pr = 7$, $Nt = Nr = Nb = 0.1$ and $Le = 10$. Regardless of the Rayleigh number the non-convective cells are formed in the streamlines along the clockwise direction inside the cavity of the figure 3.11(a). The main reason for an appearance of these circulations is an effect of the sinusoidal temperature distribution at vertical walls of the cavity. The vortices are separated by virtual horizontal and inclined wall which are both impervious and adiabatic. It can be seen from figure that there is a significant change in both the primary cells and in oval contour shape at the top side. The intensity of primary cells is decreased with the increase of Rayleigh number. The primary cells become compressed with the increase of Rayleigh number and finally turned into rectangular shape. On the other hand, the oval is large and circular in shape at bottom become thin at top side at $Ra = 10^2$. But we noticed that with the increase of Rayleigh number the oval at bottom gets smaller and top get larger gradually.

An increase of Rayleigh number there is a small change in intensity and configuration in the isotherm.

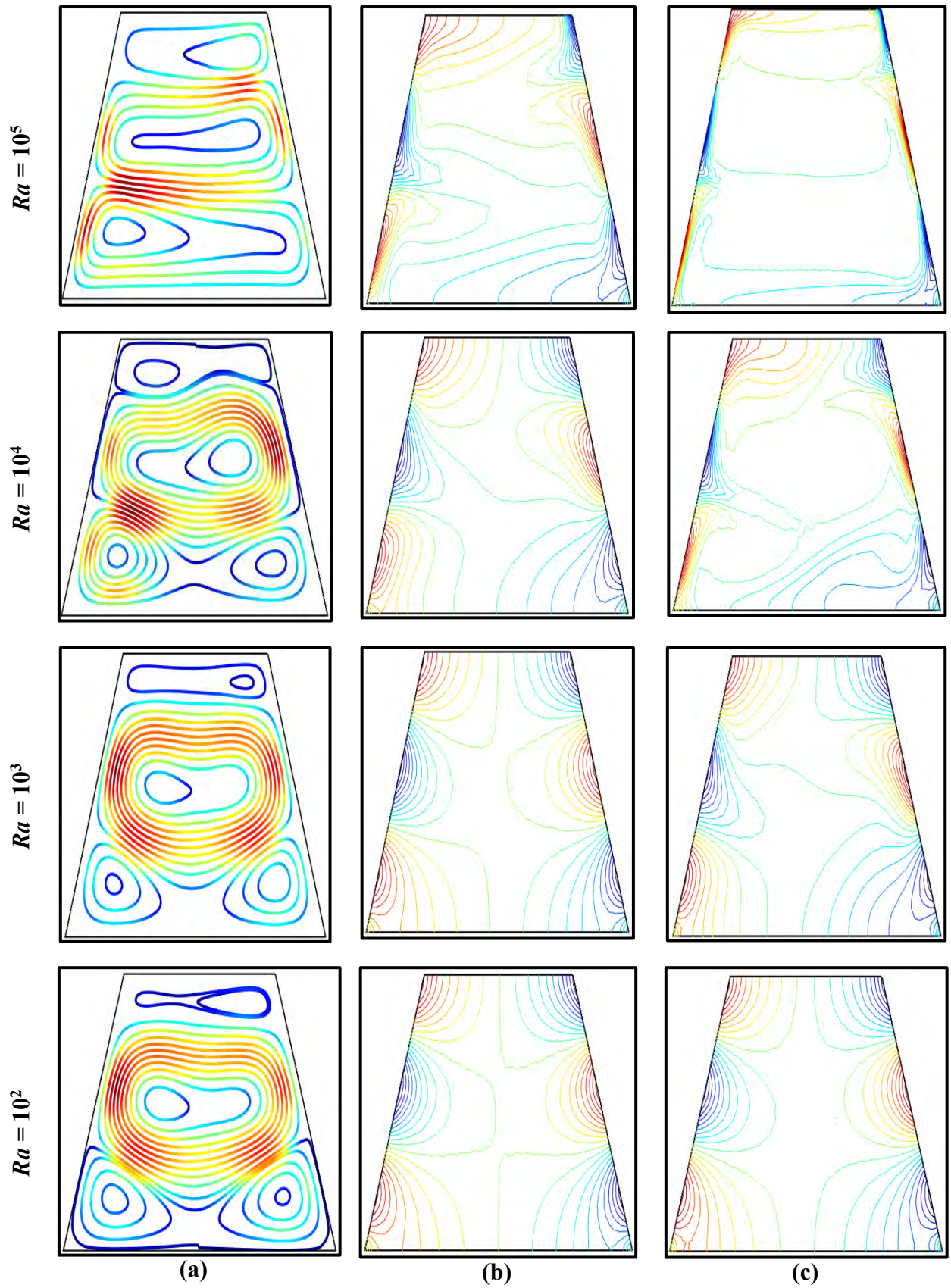


Figure 3.11: The effect of Rayleigh number on (a) streamlines, (b) isothermal lines and (c) iso-concentration lines at $Pr = 7$, $Nt = Nr = Nb = 0.1$ and $Le = 10$.

We noticed that the curve in the isotherm contour inversely changed between $Ra = 10^2$ and $Ra = 10^3$. At $Ra = 10^5$ the isothermal lines become scattered in haphazard and these distributions can be considered as non-homogeneous. The variation with the Rayleigh number is related to the iso-concentration lines is noteworthy as shown in the figure 3.11(c). Curve close to the inclined wall due to the large temperature difference in this zone. At $Ra = 10^2$ all curves are close to each other and stay in chaplet. This chaplet shape is destroyed with increasing Rayleigh number. Finally, the curves are arranged in parallel at $Ra = 10^5$.

An effect of the Rayleigh number (Ra) on the average Nusselt number at left and right inclined walls is presented in the figure 3.12. From above figure it is noticed that an increase in Rayleigh number (Ra) from $Ra = 10^2 - 10^4$, there is hardly increase in average Nusselt number. But from $Ra = 10^4$ to $Ra = 10^5$ the average Nusselt number increases are highly noticed for both left and right wall. Increasing rates of heat transfer are 36.193% and 35.988% for right and left walls, respectively. In addition, about 0.5696% enhanced rate of heat transfer is obtained for right wall than left wall.

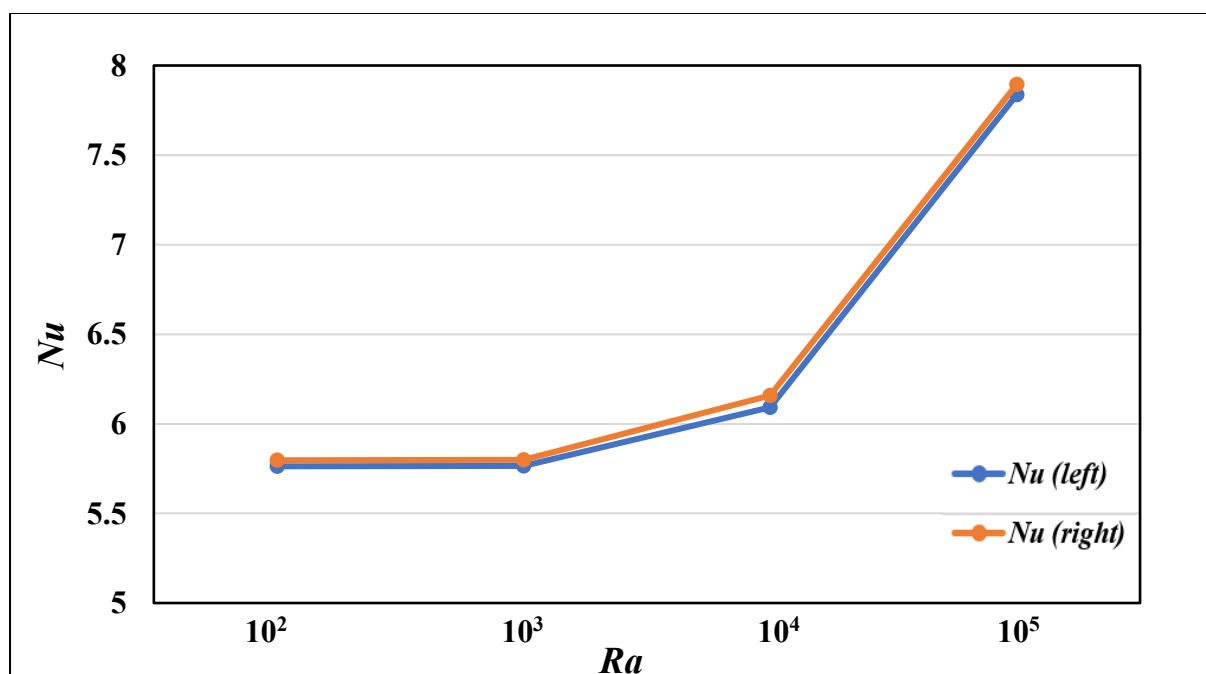


Figure 3.12: Average Nusselt Number at the left and right wall against Rayleigh number at $Le = 10$, $Ra = 10^4$ and $Nt = Nr = Nb = 0.1$.

3.8 Comparison

Three simplified test problems have been chosen for comparison, such as Demirdzic *et al.* [39] of the convective heat transfer within a parallelogram, De Vahl Davis [40] of convective

heat transfer inside a square chamber and Revnic *et al.* [5] of non-uniform border temperature variations on time-dependent nanofluid free convection within a trapezium. The present result of average Nusselt number for the variation of Prandtl and Raleigh numbers have been compared with that of the above-mentioned studies. Table 3.1 presents values of Nu along the heating halves of both inclined walls against Pr with fixed $Ra = 10^6$ and percentage of error between present result and that of Revnic *et al.* [5]. Thus, a good agreement has been observed among the present result and that of Demirdzic *et al.* [39] and Revnic *et al.* [5]. To perform this comparison the effects of other parameters have been considered as neglected.

Table 3.1: Comparison of Nu against Pr among present result and that of Demirdzic *et al.* [39] and Revnic *et al.* [5]

Pr	Nu			Error (%)
	Demirdzic <i>et al.</i> [39]	Revnic <i>et al.</i> [5]	Present result	
0.1	5.9849	5.9829	6.3568	6.25
10	7.5801	7.5847	8.0932	6.70

Similarly, Table 3.2 presents values of Nu along the heating halves of both inclined walls against Ra with fixed $Pr = 0.1$ and percentage of error between present result and that of Revnic *et al.* [5]. From the Table 3.2 it is seen that a little amount of error is found between present result and that of Revnic *et al.* [5]. Thus, for this case also, a good agreement has been observed among the present result and that of Davis and Jones [40] and Revnic *et al.* [5].

Table 3.2: Comparison of Nu against Ra among present result and that of Davis and Jones [40] and Revnic *et al.* [5]

Ra	Nu			Error (%)
	Davis and Jones [40]	Revnic <i>et al.</i> [5]	Present result	
10^3	1.116	1.121	1.189	6.06
10^4	2.234	2.306	2.401	4.12

Chapter 4: Conclusions and Recommendations

The convective free flow and heat transfer inside a trapezoidal enclosure having sinusoidal temperature distributions on both side walls have been numerically investigated using the nanofluid model proposed by Buongiorno. Mathematical model has been formulated in dimensionless mass, momentum, energy and concentration conservation forms and then solved numerically on the basis of a second-order accurate finite element method. The algorithm has been validated by direct comparisons with previously published articles.

Distributions of streamlines, isotherms, and iso-concentrations at a wide range of key parameters have been investigated. Based on the findings in this study, we conclude that the average Nusselt is increasing functions of the buoyancy-ratio parameter, thermophoresis parameter and decreasing functions of the Lewis number, Brownian motion parameter. Comparisons of the result from this numerical study have also been performed with other numerical/experimental results and the comparisons have been found to be in good agreement. The main findings of the present study have been enlisted as follows.

4.1 Conclusion

- The rate of heat transfer is obtained about 0.7081% and 0.7108% at the left and right walls, respectively for increasing values of Lewis number from 1 to 10. The increasing rate 0.3813% higher for the right wall than the left wall.
- At the right and left wall, the heat transfer rate is increased significantly at 36.37% and 35.49%, respectively with the increase of thermophoresis parameter from 0.1 to 1.5. The increase in the average Nusselt number at the right wall is 2.479% higher than the left wall.
- The increasing rate of heat transfer is obtained as 0.4104% and 0.893% at the left and right wall for increasing values of Prandtl number from 0.7 to 10.
- Variation of Brownian motion parameter from $Nb = 0.1$ to 2 leads to a significant increase in the heat transfer at the rate of 34.75% and 34.27% for the right and left walls, respectively. The average Nusselt number getting more higher about 1.40% for right wall compared with left wall.

- An increase in Nr from 0.1 to 0.7 leads to decrease in average Nusselt number. The decreasing rates of left and right wall are about 1.101% and 1.104%, respectively. After calculation the decreasing rate at right wall compared with left wall is found as 0.272%.
- Variation of Rayleigh number from $Ra = 10^2$ to 10^6 leads to a significant increase in the heat transfer rate by 36.193% and 35.988% for the right and left walls, respectively. In addition, the heat transfer rate is 0.5696% higher for the right wall than the left wall.

4.2 Future work

There is a lot of scope for research in this area in future. Since study of nanofluids is under initial stages so there is a lot of scope in development of nanofluids. The size, shape, material and volume fraction of dispersed nanoparticles play a very important role in the absorption of heat. In consideration of the present investigation, the following recommendations for future study have been provided:

- ◆ Trapezium shaped cavity has been considered in the present study. So, this deliberation may be extended by considering other formations of enclosures to investigate the performance of nanofluids.
- ◆ Using nanofluids with single phase flow have been considered as heat transfer medium in this thesis work. It can be investigated for multiphase flow also.
- ◆ In this research, Buongiorno's nanofluid model has been used. Anyone can use other nanofluid model to obtain better heat transfer rate.

References

- [1] H.M. Elshehabey, S.E. Ahmed, “MHD mixed convection in a lid driven cavity filled by a nanofluid with sinusoidal temperature distribution on the both vertical walls using Buongiorno’s nanofluid model”, *International Journal of Heat and Mass Transfer*, Vol. 88, pp. 181-202, 2015.
- [2] M. Sheikholeslami, M. Gorji- Bandpy, D.D. Ganji, P. Rana, S. Soleimani, “Magneto hydrodynamic free convection of Al_2O_3 -water nanofluid considering thermophoresis and Brownian effects”, *Computer and Fluids*, Vol. 94, pp.147-160, 2014.
- [3] P. Suriyakumar, A. Devi, “Buongiorno Model for hydromagnetic convection flow of nanofluid over an inclined stretching surface with variable stream conditions”, *Journal of Advanced research in Applied Mechanics and Computational Fluid Dynamics*, Vol. 6, pp. 1-14, 2019.
- [4] A. Falana, O.A. Ojewale, T.B. Adeboje, “Effect of Brownian motion and thermophoresis on a nonlinearly stretching permeable sheet in a nanofluid”, *Advances in Nanoparticles*, Vol. 5, pp. 123-134, 2016.
- [5] C. Revnic, M. Ghalambaz, T. Grosan, M. Sheremet, I. Pop., “Impact of non-uniform border temperature variations on time-dependent nanofluid free convection within a trapezium: Buongiorno’s nanofluid model”, *Energies*, Vol. 12, pp. 1-14, 2019.
- [6] A. Esfandiary, B. Mehmandoust, A. Karimipour, H.A. Pakravan, “Natural convection of Al_2O_3 -water nanofluid in an inclined enclosure with the effect of slip velocity mechanism: Brownian motion and thermophoresis phenomenon”, *International journal of Thermal Science*, Vol. 105, pp. 137-158, 2016.
- [7] H. Zargartalebi, M. Ghalambaz, A. Noghrehabadi and A. Chamkha, “Natural convection in an enclosure within inclined local thermal non-equilibrium porous fin considering Buongiorno’s model”, *An International Journal of computer and Methodology*, Vol. 70, pp. 432-445, 2016.

References

- [8] M.S. Alam, F. Sarower, M.M. Rahman, M.J. Uddin “Effect of thermophoresis and Brownian motion on unsteady forced convection flow of a nanofluid along a porous wedge with variable suction”, *Bulletin of Calcutta Mathematical Society*, Vol. 107, pp. 393-410, 2015.
- [9] A. A. Samimi Behbahan, I. Pop, “Thermophoresis and Brownian effects on natural convection of nanofluids in a square enclosure with two pairs of heat source/sink”, *International Journal of Numerical Methods for Heat & Fluid Flow*, Vol. 25, pp. 1030-1046, 2015.
- [10] M.A. Sheremet, T. Grosan, I. Pop “Free convection in a shallow and slender porous cavity filled by a nanofluids using Buongiorno’s model”, *ASME Journal of Heat Transfer*, Vol. 136, pp. 082-501, 2014.
- [11] H.M. Elshehabeey, S.E. Ahmed, “MHD mixed convection in a lid driven cavity filled a nanofluid with sinusoidal temperature distribution on the vertical walls using Buongiorno’s nanofluid model”, *International journal of heat and Mass Transfer*, Vol. 88, pp. 181-202, 2015.
- [12] Z. Haddad, E. Abu-nadac, H.F. Oztop, A. Mataoui, “Natural convection in nanofluids: are the thermophoresis and Brownian motion effects significant in nanofluid heat transfer enhancement”, *International Journal of Heat and Mass Thermal science*, Vol. 57, pp. 152-162, 2012.
- [13] M.H. Matin, B. Ghanbari, “Effect of Brownian motion and thermophoresis on the mixed convection of nanofluid in a porous channel including flow reversal”, Vol. 101, pp. 115-136, 2014.
- [14] H. Aminfar, M.R. Haghgoo, “Brownian motion and thermophoresis effects on natural convection of alumina-water nanofluid”, *Journal of Mechanical, Engineering and Science* Vol. 6, pp. 1-11, 2012.
- [15] A.I. Alsabery, A.j.Chamkhab, H. salehd, I. Hashima, B. Chananee, “Effect of spatial side-wall temperature variations on transient natural convection of a nonofluid in a traphezoidal cavity”, *International Journal of Numerical Methods Heat Fluid Flow*, Vol. 27, pp. 1365-1384, 2017.
- [16] M.A. Sheremet, I. Pop “Natural convection in square porous cavities with sinusoidal temperature distribution on both side walls filled with a nanofluid: Buongiorno’s

References

- model”, *Transparent porous medium*, Vol. 105, pp. 411-429, 2014.
- [17] S. Sivasankaran, M. Bhuvaneshwari, “Natural convection in porous cavity with sinusoidal heating on both sidewalls”, *Numerical Heat Transfer Part A*, Vol. 63, pp. 14-30, 2013.
- [18] C.J. Ho, W.K. Liu, Y.S. Chang, C.C. Lin, “Natural convection heat transfer of Alumina-water nanofluid in vertical square enclosure”, *International Journal of Thermal science*, Vol. 49, pp. 1345-1353, 2010.
- [19] A. Malvandi, S. Heysiattalab, D.D. Ganji, “Thermophoresis and Brownian motion effect on heat transfer enhancement at film boiling of nanofluids over a vertical cylinder”, *Journal of Molecular Liquids*, Vol.216, pp. 503-509, 2016.
- [20] F. Garoosi, L.Jahanshaloo, M.M. Rashidi, A. Badakhsh, M.E.Ali, “Numerical Simulation of natural convection of the nanofluid in heat exchangers using a Buongiorno model”, *Applied Mathematics and Computation*, Vol. 254, pp. 183-203, 2015.
- [21] F. Garoosi, S. Garoosi, K. Hooman, “Numerical simulation of natural convection and mixed convection of the nanofluid in a square cavity using Buongiorno model”, *Powder Technology*, Vol. 268, pp. 268-292, 2014.
- [22] R. O. Sayyar, M. Saghafian, “Numerical simulation of convective heat transfer of non-homogeneous nanofluid using Buongiorno’s model”, *Heat and Mass Transfer*, Vol. 53, pp. 2627-2636, 2017.
- [23] A. Malvandi, D.D. Ganji, “Brownian motion and thermophoresis effects on slip flow of Alumina water nanofluid inside a circular microchannel in the presence of a magnetic field”, *International Journal of Thermal Sciences*, Vol. 84, pp. 196-206, 2014.
- [24] S. Kata, S. Ganganapall, V. Kuppalapalle, “Effect of thermophoresis and Brownian motion on the melting heat transfer of a Jeffrey fluid near a stagnation point towards a stretching surface: Buongiorno's model”, *Article*, Vol. 48, pp. 3328-3349, 2019.
- [25] M. Qasim, Z.H. Khan, R.J. Lopez, W.A. Khan, “Heat and mass transfer in nanofluid thin film over an unsteady stretching sheet using Buongiorno’s model”, *The European Physical. Journal Plus*, Vol. 16, pp.131, 2016.

References

- [26] I. Pop, M. Ghalambaz, M. Sheremet, “Free convection in a square porous cavity filled with a nanofluid using thermal non equilibrium and Buongiorno models”, *International Journal of Numerical Methods for Heat and Fluid Flow*, Vol. 26, pp. 671-693, 2016.
- [27] H. Zargartalebi, M. Ghalambaz, A. Noghrehabadi, A. J. Chamkha, “Natural convection of a nanofluid in an enclosure with an inclined local thermal non-equilibrium porous fin considering Buongiorno’s model”, *International Journal of Computation and Methodology*, Vol. 70, pp. 432-445, 2016.
- [28] A. Noghrehabadi, A. Behseresht, M. Ghalambaz, “Natural convection of nanofluid over vertical plate embedded in porous medium: Prescribed surface heat flux”, *Applied Mathematics and Mechanics*, Vol. 34, pp. 669-686, 2016.
- [29] R. Onsor Sayyar, M. Saghafian, “Numerical simulation of convective heat transfer of nonhomogeneous nanofluid using Buongiorno model”, *Heat and Mass Transfer*, Vol 53, pp. 2627–2636, 2017.
- [30] H. Saleh, R. Roslan., I. Hashim, “Natural convection heat transfer in a nanofluid-filled trapezoidal enclosure”, *International Journal of Heat and Mass Transfer*, Vol. 54, pp. 194-201, 2011.
- [31] S. Soleimani, M. Sheikholeslami, D.D. Ganji, M. Gorji-Bandpay, “Natural convection heat transfer in a nanofluid filled semi-annulus enclosure”, *International Communications in Heat and Mass Transfer*, Vol. 39(4), pp. 565-574, 2012.
- [32] M.A Sheremet., T. Groşan, I. Pop, “Steady-state free convection in right-angle porous trapezoidal cavity filled by a nanofluid: Buongiorno’s mathematical model”, *European Journal of Mechanics-B/Fluids*, Vol. 53, pp. 241-250, 2015.
- [33] F. Garoosi, L. Jahanshaloo, M.M. Rashidi, A. Badakhsh, M.E. Ali “Numerical simulation of natural convection of the nanofluid in heat exchangers using a Buongiorno model”, *Applied Mathematics and Computation*, Vol. 254, pp. 183-203, 2015.
- [34] S.M. Al-Weheibi, M.M. Rahman, M.S. Alam, K. Vajravelu, “Numerical simulation of natural convection heat transfer in a trapezoidal enclosure filled with nanoparticles”, *International journal of Mechanical Science*, Vol. 131, pp. 599-612, 2017.

References

- [35] M.H. Esfe, A.A.A. Arani, W.M. Yan, H. Ehteram, A. Aghaie, M. Afrand, “Natural convection in a trapezoidal enclosure filled with carbon nanotube–EG–water nanofluid”, *International Journal of Heat and Mass Transfer*, Vol. 92, pp. 76-82, 2016.
- [36] P.F. Alvarino, J. S. Jabardo, A. Arce, M.L. Galdo, “A numerical investigation of laminar flow of a water/alumina nanofluid”, *International Journal of Heat Mass Transfer*, Vol. 59, pp. 423–432, 2013.
- [37] R. V. Ramachandra, R. M. Suryanarayana, “Heat and Mass transfer analysis of Buongiorno's model nanofluid over linear and non-linear stretching surface with Thermal radiation and Chemical reaction”, *Research Journal of Pharmacy and Technology*, Vol. 11, pp. 4527-4533, 2018.
- [38] J.A. Khan, M. Mustafa, T. Hayat, M. Turkyilmazoglu, A. Alsaedi, “Numerical study of nanofluid flow and heat transfer over a rotating disk using Buongiorno’s model”, *International Journal of Numerical Methods for Heat & Fluid Flow*, Vol. 27, pp. 221-234, 2017.
- [39] I. Demirdzic, Z. Lilek, M. Peric, “Fluid flow and heat transfer test problems solutions for non- orthogonal grids: Benchmark”, *International Journal of Numerical Methods Fluids*, Vol. 15, pp. 329–354, 1992.
- [40] G. De Davis, I.P. Jones, “Natural convection in a square cavity: A bench mark numerical solution”, *International Journal of Numerical Methods Fluids*, Vol. 3, pp. 227–248, 1983.
- [41] K. Venkatadri, SA. Gaffar, VR. Prasad, BHM. Khan, OA. Beg, “Simulation of natural convection heat transfer in a 2-D trapezoidal enclosure”, *International Journal of Automotive and Mechanical Engineering*, Vol. 16, pp. 7375-7390, 2019.
- [42] J. Buongiorno, “Convective transport in nanofluids”, *ASME Journal of Heat Transfer*, Vol. 128, pp. 240-250, 2006.
- [43] Mohammad Ali, M.A. Alim, R. Nasrin, M.S. Alam, M.J.H. Munshi, “Similarity solution of unsteady MHD boundary layer flow and heat transfer past a moving wedge in a nanofluid using the Buongiorno model”, *Procedia Engineering*, Vol. 194, No. C, pp. 407-413, 2017.

References

- [44] M.S. Rahman, R. Nasrin, M.I. Hoque, “Heat-mass transfer of nanofluid in lid-driven enclosure under three convective modes”, *GANIT Journal*, Vol. 38, pp. 73-83, 2018.
- [45] R. Nasrin, M.A. Alim, Ali J. Chamkha, “Effect of heating wall position on forced convection along two-sided open enclosure with porous medium utilizing nanofluid”, *International Journal of Energy & Technology*, Vol. 5(9), pp. 1-13, 2013.
- [46] Ishrat Zahan, R. Nasrin, M.A. Alim, “MHD effect on conjugate heat transfer in a nanofluid filled rectangular enclosure”, *International Journal of Petrochemical Science and Engineering*, Vol. 3, pp. 114-123, 2018.
- [47] P. Dechaumphai, “Finite Element Method in Engineering”, 2nd edition, Culalongkorn University Press, Bangkok, 1999.
- [48] C. Taylor, P. Hood, “A numerical solution of the Navier-Stokes’s equations using finite element technique”, *Computer and Fluids*, Vol. 1, pp. 73–89, 1973.